Functional genomics in chicken embryos reveal the pathogenicity of two missense FZD2 variants associated with dominant Robinow syndrome

Shruti S. Tophkhane[1], Katherine Fu[2], Joy M. Richman [1*]

Life Sciences Institute and Faculty of Dentistry, University of British Columbia, Vancouver, V6T 1Z3, Canada

***To whom correspondence should be addressed at:** Life Sciences Institute, 2350 Health Sciences Mall, University of British Columbia Vancouver, BC, V6T 1Z3, Canada. Tel: 604 822 3568; Fax: 604 822 2316; Email: richman@dentistry.ubc.ca

Key words: Intramembranous ossification, micromass cultures, RCAS, WNT signaling, luciferase assays

ABSTRACT

Robinow syndrome (RS) is a rare, genetically heterogeneous condition caused by mutations in seven WNT pathway genes. The clinical presentation includes craniofacial widening and jaw hypoplasia. Here we tested the functional impact of two missense *FZD2* variants in the frontonasal mass in the chicken embryo, the area homologous to the affected region in RS. Viruses coding for wild-type or variant forms of FZD2 (code for P142L and G434V) inhibited beak ossification in vivo and certain bones failed to differentiate, possibly mediated by decreased levels of *CTNNB1* and abnormal BMP signaling. In primary cultures, variants of FZD2, inhibited chondrogenesis, caused increased nuclear shuttling of β-catenin and increased expression of early mesenchyme marker, TWIST which precedes chondrocyte specification. To determine the impact of the variants on WNT pathways we used luciferase reporters. The G434V and P142L plasmids dominantly interfered with wtFZD2 in SuperTopflash canonical assays. The P142L variant repressed the activity of the ATF2 reporter in the presence of the *Ror2* co-receptor. This is the first study to show that the missense variants in *FZD2* have functional defects and that the upper face skeletal defects in chickens recapitulate features of the jaw hypoplasia and flat profile of people with Robinow Syndrome.

INTRODUCTION:

Multiple syndromes include craniofacial dysmorphology as part of the clinical presentation. Studying the syndrome causing mutations sheds light on gene function in many aspects of facial morphogenesis, patterning and differentiation. Our disease model in this study is Robinow syndrome (RS), a rare skeletal dysplasia syndrome (1:500,000 live births) that primarily affects the skeleton of the face and limbs (Mazzeu and Brunner, 2020). RS was first reported in 1969 in a family with dwarfism and "fetal facies" (Robinow et al., 1969). Currently, seven genes from the Wingless-related Integration site 1 (WNT) pathway are linked with the pathogenesis of RS. Of these, Receptor tyrosine kinase-like orphan receptor 2 (*ROR2*) and Nucleoredoxin (*NXN)* cause autosomal recessive disease (Zhang et al., 2022; White et al., 2018) while Dishevelled (*DVL1*, *DVL2*, *DVL3)*, *WNT5A*, Frizzled2 (*FZD2*) have autosomal dominant inheritance (Table S1)(Zhang et al., 2021; White et al., 2018; Nagasaki et al., 2018; White et al., 2016; White et al., 2015; Person et al., 2010). Individuals affected with RS present with dysmorphic facial features (hypertelorism or wide-spaced eyes, broad forehead, flat nasal bridge)(Conlon et al., 2021; Beiraghi et al., 2011), mesomelic limb shortening (Zhang et al., 2022; Abu-Ghname et al., 2021), and genital abnormalities (Roifman et al., 2019; Patton and Afzal, 2002). Despite high genetic heterogeneity, RS individuals have similar clinical presentations (Mazzeu et al., 2007) which suggests that ultimately the genes may share a common, indirect, downstream mediator. Previously we examined the WNT5A variants in jaw development (Hosseini-Farahabadi et al., 2017)and here we are focusing on *FZD2* variants and how they affect craniofacial patterning and skeletogenesis.

WNTs are secreted glycoproteins that trigger multiple intracellular pathways – (i) canonical or β-catenin-dependent (Rim et al., 2022; Nusse and Clevers, 2017) and (ii) several non-canonical or β-catenin-independent pathways (Riquelme et al., 2023; Rogers and Scholpp, 2022; Lojk and Marc, 2021; Angers and Moon, 2009). All the genes implicated in RS act in the non-canonical, c-Jun Planar Cell Polarity (JNK/PCP) pathway which is triggered by WNT ligands such as WNT5A binding to ROR2 homodimers or ROR2-FZD heterodimers (Stricker et al., 2017). Activation leads to increased Rho GTPase activity and JNK signaling, ultimately affecting cell shape and migration. In RS several genes also operate in the canonical WNT pathway (*FZD2* and *DVL1,2,3*). Therefore the pathogenesis of RS could result from an imbalance of multiple WNT signaling pathways as we recently reported for *DVL1* mutations (Gignac et al., 2023) and others reported for *FZD2* loss-of-function mutations (Zhu et al., 2023; Liegel et al., 2023).

WNT ligand binds with *FZD* and Low-density lipoprotein receptor-related protein5/6 (*LRP5/6*) receptors to activate the canonical/β-catenin-dependent pathway via phosphorylation and activation of *DVL*. The *FZD/LRP/DVL* complex destabilizes the β-catenin destruction which increases cytoplasmic accumulation of β-catenin. Free β-catenin is then translocated into the nucleus, where it forms a complex with the T-cell factor/Lymphoid Enhancer Factor (TCF/LEF) family of transcription factors, replacing the transcriptional inhibitor Groucho, and activates transcription of WNT target genes (Nusse and Clevers, 2017). The translocation of β-catenin to the nucleus is a major signaling step in the WNT pathway and is often used as a read out of active canonical pathway (Anthony et al., 2020; Valenta et al., 2012). Conditional loss-of-function of β-catenin (*Ctnnb1*) in mice causes severe defects in nasal, upper jaw, and ocular structures resembling holoprosencephaly (Wang et al., 2011). The transcriptional targets of CTNNB1, $Lef^{-/-}/Tcf^{-/-}$, were also knocked out and these mice presented with narrow faces (Brugmann et al., 2007). This lack of correlation of phenotypes of RS compared to the mouse mutants indicates that a closer examination of missense variants in functional assays is needed.

FZD2 is a member of the G protein-coupled receptor (GPCRs) superfamily (Zhao et al., 1995) and is expressed abundantly in the craniofacial tissues during embryogenesis (Yu et al., 2012; Yu et al., 2010; Geetha-Loganathan et al., 2009). The extracellular region of all FZDs consists of a N-terminal signal sequence followed by a highly conserved cysteine-rich domain (CRD) essential for WNT ligand binding. The CRD is linked to the 7-pass transmembrane domain consisting of three extra- and three-intracellular loops and a C-terminus. The third intracellular loop and C-terminus are essential for interaction with Dishevelled (Zhu et al., 2023; Tauriello et al., 2012). There are 10 *FZD* receptors ($FZD_{1\text{-}10}$) in mammals with redundant functions. *FZD1*, *2*, and *7* share 75% sequence homology and display substantial redundancy expression and function multiple developmental processes (Yu et al., 2012; Yu et al., 2010). Fz2 is required for the Wnt3a-dependent accumulation of β-catenin and Wnt5a competes with Wnt3a for binding to Fz2 in vitro, thereby inhibiting the β-catenin pathway (Sato et al., 2010). $Fzd2^{-/-}$ (Saal et al., 2015; Yu et al., 2010), homozygous, frameshifted mice (Zhu et al., 2023) and mice with nonsense mutations in Fzd2 (Liegel et al., 2023) are born with cleft palate suggest that *Fzd2* plays crucial roles in craniofacial development. $Fzd2^{-/-}$ mice have severe craniofacial defects while individuals with *FZD2*-associated ADRS have mild phenotypes (Zhang et al., 2021), therefore other animal models that model more closely the RS features are needed.

In this study we are investigating missense *FZD2* variants using a model organism, the chicken embryo. The missense *FZD2* variants (c.1301G>T, p.Gly434Val; c.425C>T, p.Pro142Leu) were chosen based on their location in the gene (one extracellular and one intracellular), unclear pathogenicity and severity of facial phenotypes. The P142L variant lies in the CRD (Fig. S1A,B,B') and was detected in a compound heterozygous individual (p.Pro142Leu, p.Trp377*)(White et al., 2018). The father and two siblings of the proband also possessed the P142L variant and have short stature but no obvious facial differences. The mother of the proband carries truncating mutation in *FZD2* (Trp377*) and presents with face and limb defects. Since the genotype-phenotype correlation is undetermined, P142L is considered a variant of uncertain significance (White et al., 2018). The second variant G434V (c.1301G >T) has been linked with majority of ADRS-*FZD2* cases and is termed "likely pathogenic" as it correlates with most severe phenotypes. Glycine 434 is highly conserved and present in the third intracellular loop of *FZD2* (Fig. S1A,C,D), a region that is essential for dishevelled binding and WNT signaling (Tauriello et al., 2012). In silico modeling of the G434V mutation resulted in severe steric hindrance along with mutation in configuration of *FZD2* protein (Türkmen et al., 2017) (Fig. S1C,D). Previously, the G434V variant was associated with pathogenesis of autosomal dominant Omodysplasia type II (OMODII)(Zhang et al., 2021; Nagasaki et al., 2018; Warren et al., 2018; Türkmen et al., 2017; Saal et al., 2015). Since many aspects of Omodysplasia overlap RS, the G434V variant is now considered to be part RS disease causing variations (Liegel et al., 2023; Zhang et al., 2022).

While mouse models provide valuable information about gene function, particularly loss-of-function mutations, it is challenging to knock-in specific single nucleotide, missense variants. We use the chicken embryo which is a time and cost-effective animal model to study missense variants associated with dominant disease. Moreover, the chicken embryo allows 3D morphogenesis of the beak to take place up to full skeletogenesis. Our strategy was to misexpress retroviruses carrying the human *FZD2* or *GFP* control gene inserts by injecting into the frontonasal mass (Fig. 1A). The frontonasal mass in birds forms the prenasal cartilage and the flanking premaxillary intramembranous bones (Abramyan and Richman, 2018) and is homologous to the human facial midline (bridge of nose, centre of nose, nasal septum, philtrum and centre of upper lip plus premaxilla). The observed phenotypes caused by the variant forms of FZD2 are compared to the wild-type gene to tease apart unique functions of the variants (Gignac et al., 2023; Gignac et al., 2019; Hosseini-Farahabadi et al., 2017). Here, we uncover new functional evidence that the P142L

variant is pathogenic both in cell differentiation and in 2 WNT signaling pathways. The G434V variant inhibits chondrogenesis, functions normally in the JNK-PCP pathway but acts as a dominant-negative receptor in the canonical WNT pathway.

RESULTS

In these experiments we compare the effects of generalized increased levels of *FZD2* to the *GFP* control and viruses coding for the two FZD variants (P142L and G434V). GFP viruses do not affect development (Hosseini-Farahabadi et al., 2017; Geetha-Loganathan et al., 2014). The strategy used here is to express the human genes in defined regions of the developing organism, alongside the endogenous wild-type alleles. This design suitable for studying autosomal dominant mutations that are thought to cause an interference between mutant and wild-type protein. Indeed, our previous work on an autosomal dominant DVL1 frameshift mutations (Gignac et al., 2023) and *WNT5A* missense mutations (Gignac et al. 2019; Hosseini-Farahabadi et al. 2017) found evidence for dominant interference that reduced bone size and changed bone shape. *FZD2* is ubiquitously expressed in the face in chicken and mouse (Saal et al., 2015; Yu et al., 2012; Yu et al., 2010; Geetha-Loganathan et al., 2009). If the proteins coded by missense *FZD2* variants expressed on top of the Gallus *FZD2* lacked function, then the upper beak of the mutant *FZD2* viruses should look like *GFP* controls. If the mutations caused no additional effects other than those caused by overexpression of *FZD2*, then phenotypes are due to generally higher levels of *FZD2* rather than specific effects of the variants. If the phenotypes were similar but more severe than wt*FZD2*, then the variants caused a gain-of-function. Finally, if the mutant viruses induced de novo phenotypes compared to wt*FZD2*, then this would suggest more complex functional alterations that would require additional analysis.

Human *FZD2* viruses inhibit patterning and ossification of frontonasal mass derivatives in chicken embryo

The majority of embryos infected with viruses coding for wtFZD2 or mutant FZD2 had normal external beak morphology (Table S2) and survivorship ranged between 64-78% (Table S3). In cleared embryos, GFP infected skulls all frontonasal mass derivatives were present and fully ossified (Fig. 1C-C’’; Fig. S2A-C). The spread of the GFP virus in the upper beak confirmed accurate targeting (Fig. 1C’ inset). Decreased bone staining and agenesis of bones were observed in majority of embryos (Fig. 1B) particularly the absence of the prefrontal and/or the nasal bone (wtFZD2, 80%; P142L, 69%; G434V, 84%; Fig. 1D-F’’; Fig. S2D-L; Table S2). These results suggested that having generally higher levels of exogenous FZD2 protein, whether normal or variant, inhibits intramembranous formation.

Misexpression of *FZD2* has no effect on early stages of development

To understand the mechanism for the skeletal phenotypes we examined embryos prior to the onset of differentiation, at stage 28. Using qRT-PCR we verified presence of the human *FZD2* (h*FZD2*) with human specific primers (Fig. 2I; Table S8). The virus is not evenly expressed at stage 28 which explains the increased variability qRT-PCR results (Fig. 2I,J). While the levels of expression of the exogenous genes were above physiological levels, the levels of the Gallus *FZD2* RNA were unchanged (Fig. 2J). This is important as we can rule out a decrease in the level of Gallus RNA mediating the phenotypes. There are likely normal levels of Gallus FZD2 protein expressed in the presence of the variants.

Embryos were sectioned and near-adjacent sections stained with antibodies to confirm the location of the retroviruses. Antibodies to viral GAG protein confirmed that virus was correctly targeted to the centre of the frontonasal mass with the spread of the virus being variable (Fig. 2A,B,C,D). We therefore selected embryos with strong medial expression for further molecular characterization. Serial sections were stained with the chondrogenic marker SOX9 (SRY-Box Transcription Factor 9) and TWIST1, a marker for undifferentiated mesenchymal cells. The viruses expressing FZD2 protein, did not affect the differentiation of SOX9-positive prenasal cartilage (Fig. 2A',B',C',D'). The TWIST-positive undifferentiated mesenchyme was also unaffected (Fig. 2A'', B'', C'', D''). We examined tissues from viral infected animals using an antibody to β-catenin phosphorylated at Try 489 which shows the nuclear shuttling of β-catenin protein. Increased nuclear localization of β-catenin protein was induced by all FZD2 viruses compared to GFP controls (Fig. 2E-H'). The percentage of nuclei positive for β-catenin protein was significantly increased in the P142L variant (Fig. 2K) suggesting possible activation of canonical WNT signalling. We also analyzed cell proliferation (BrdU) (Fig. 2A'''-D'''; Table S4) and apoptosis (TUNEL; Fig. S3A-D) at stage 28 to determine if there were fewer cells giving rise to the beak skeleton. However, there were no detectable differences in cell dynamics between the viruses coding for GFP or FZD2.

Since WNT and Bone Morphogenic Protein (BMP) pathway mediate osteogenesis independently and synergistically, we measured the levels of WNT and BMP pathway mediators with qRT-PCR. All comparisons were made to control GFP. At stage 28, Gallus *FZD2* (g*FZD2*) levels were not changed as a result of the exogenous human gene (Fig. 2J). Notably, in all human *FZD2* virus-infected frontonasal mass tissue, *CTNNB1* and the non-canonical WNT receptor

ROR2 were significantly downregulated at stage 28 compared to *GFP* (Fig. 2J) suggesting impairment of both canonical and non-canonical WNT signaling. Loss-of-function mutations in *ROR2* cause autosomal recessive RS (Table S1). Thus, indirect down-regulation of ROR2 by FZD2 could contribute to the similarity in phenotypes. In the BMP pathway, the P142L variant significantly downregulated *BMP2*, *BMP7*, *NOGGIN*, and *BMPER*, while G434V variant downregulated *BMP2* and *BMPER* (Fig. 2J). The decrease in *BMPER* by all forms of viruses is intriguing since the BMPER protein can either increase or decrease BMP signaling, depending on the context (Correns et al., 2021). Less BMP signaling could result in decreased membranous bone formation. Thus, the synergistic downregulation of WNT canonical and non-canonical pathway mediators plus altered BMP pathway mediators may together disrupt chondrogenesis.

Mutant *FZD2* viruses inhibit chondrogenesis in frontonasal mass micromass cultures

Since BMP pathway gene expression was affected in vivo, and this pathway is known for regulating chondrogenesis, we turned to high density primary cultures derived from the frontonasal mass to study chondrogenesis. Micromass cultures are a well-established approach to study chondrogenesis in the face (Hosseini-Farahabadi et al., 2013; Richman and Crosby, 1990) and limb (Weston et al., 2002). GFP-infected control cultures showed strong green fluorescence on day 4, 6 and 8 (Fig. S4A,J,S). Viruses expressing human *FZD2* were detected using qRT-PCR in day 6 and 8 cultures (Fig. 3Y). The high levels of human virus did not change the expression endogenous genes such as gallus *FZD2* (Fig. 3Z). All viruses allowed formation of Alcian blue stained cartilage matrix on day 4 (Fig. S4B-E; and in sections F-I) suggesting there are no changes in the earliest cartilage condensations. At day 6, mineralization in the cartilage was first visible (Fig. S4K-N) and robust cartilage sheets formed in the centre for all viruses (Fig. 3A-D; Fig. S4O-R). By day 8 mineralization had progressed and there did not appear to be qualitative differences in staining (Fig. S4T-W'). In histological sections the cultures were thinner and had less cartilage in all the *FZD2*-infected specimens compared to *GFP* (Fig. 3M-P; AB, AC; Fig. S4X-AA).

In order to verify viral expression and molecular changes in micromass cultures, we studied the sections of paraffin embedded cultures with immunostaining. All day 6 and 8 cultures exhibited strong GAG and FLAG staining confirming presence of FZD2, Flag-tagged protein (Fig. 3E-H; Q-T). Adjacent sections showed type II collagen (Fig. 3I-L). On day 8, histological sections showed that all *FZD2*-infected cultures had less type II collagen (Fig. 3U-X; AC). We measured cell proliferation and apoptosis since the thickness of the cultures was affected. There was no

difference in TUNEL-positive cells on day 6 or day 8 (Fig. S3E-N) or in BrdU staining for cells in S-phase (Fig. S5A-H). Therefore, the likely reason for the reduced thickness of the cultures was a deficiency in extracellular matrix.

SOX9 regulates *COL2A1* in chondrocytes (Ng et al., 1997; Bell et al., 1997). We used a SOX9-luciferase reporter (Weston et al., 2002) to measure SOX9 transcriptional activity in the earliest stages of chondrocyte specification (2 days after plating the cultures condensations are visible) (Bi et al., 1999). The *P142L* variant virus fails to activate the reporter (Fig. 3AD). This suggests that the delay in SOX9 expression could reduce the number of cells specified to become chondrocytes. Ultimately fewer chondrocytes would contribute to lower cartilage matrix deposition in day 8 P142L-infected cultures.

Prolonged TWIST expression is seen in mutant *FZD2*-infected cultures

To investigate the possible role of canonical WNT signaling in mediating the chondrogenic phenotypes of FZD2 infected cultures, we examined expression of nuclear β-catenin, a marker of active canonical WNT signaling. On day 8, in GFP and wtFZD2 infected cultures, majority of β-catenin positive cells were present at the periphery of the cultures and excluded from the cartilage. In contrast, in *P142L* and *G434V*-infected cultures, chondrocytes had β-catenin-positive nuclei (Fig. 4E-H',M). To measure the activity of the canonical WNT pathway in the virus-infected cultures we used SuperTopflash (STF) luciferase reporter (Biechele and Moon, 2008). Optimal timing of transfection of reporters is at 48h, just when condensations for cartilage are forming. At these early stages, canonical signaling was significantly higher activity in cultures infected with both variants compared to wtFZD2 and control GFP (Fig. 4N) which correlates with higher nuclear β-catenin expression (Fig. 4M).

In cranial mesenchyme β-catenin was shown to bind with the 5′ enhancer element upstream of the promoter of Twist1 (Goodnough et al., 2012). Therefore, as another readout of the β-catenin pathway, we examined if chondrocytes expressed TWIST1. TWIST1+ nuclei were more abundant in the P142L and G434V variants to GFP (Fig. 4I-L',O). Thus, FZD2 variants cause β-catenin to enter the nucleus which in turn may activate chondrogenic repressor TWIST in vitro.

***FZD2* variants have dominant-negative effects on wt*FZD2* function**

To clarify the activity levels of canonical and non-canonical WNT signaling, plasmids containing wt*FZD2* or *FZD2* variants were transiently transfected in frontonasal mass micromass cultures (to maintain experimental consistency in expression levels and cell context) or in

HEK292T cells (commonly used for luciferase assays). Plasmids allowed more precise timing and levels of expression of transgenes in the cells. The retroviruses gradually increase expression due to lateral and vertical transmission.

The insertion of wt*FZD2* plasmid strongly activated STF in frontonasal mass cultures compared to control plasmid (Fig. 5A). In contrast WNT/β-catenin activity in the *FZD2* variants was significantly lower compared to wt*FZD2* (Fig. 5A). This suggested that the human *FZD2* can activate canonical pathway by utilizing endogenous ligands present in facial mesenchyme. To test the role of canonical WNT ligand, the cultures were supplemented with exogenous hWNT3A protein. The addition of WNT3A strongly activated the reporter and this level was unaffected by the presence of the plasmids (Fig. 5B). In HEK293 cells, wt*FZD2* induced STF activity while both *FZD2* variants showed loss-of-function (Fig. 5C; similar to frontonasal mass cultures). When WNT3A was added, there was similar activation of the pathway, regardless of which plasmid was transfected (Fig. 5D,G).

FZD receptors form multimers in the cell membrane (Carron et al., 2003; Dann et al., 2001) therefore we next added equimolar amounts of wt*FZD2* with each of the variants to mimic the heterozygous, autosomal dominant genotype of RS individuals. Both variants showed significant dominant-negative effects on the activity of wt*FZD2* (Fig. 5E,H). Since the G434V mutation lies in the DVL-binding domain, we combined *FZD2* plasmids with those expressing wt*DVL1*. All *FZD2* plasmids combined with wt*DVL1* significantly activated canonical reporter compared to wt*DVL1* alone (Fig. 5F). This showed that the variants do not interfere with DVL1-FZD2 interaction. Our data showing dominant negative effects on canonical WNT signaling (Fig. 5H) is consistent with a study that found that a different RS-associated *FZD2* variant ($FZD2^{W548*}$) decreases canonical WNT signaling (Liegel et al., 2023).

Extracellular P142L mutation had reduced ligand and co-receptor binding capacity the caused a loss-of-function in the JNK/PCP pathway

Since *FZD2* is known to participates in both canonical and non-canonical WNT pathways (Komiya and Habas, 2008; Gordon and Nusse, 2006), we used activating transcription factor 2 (ATF2)-luciferase (Ohkawara and Niehrs, 2011) to measure the JNK-PCP pathway activity. When the micromass cultures were transfected with wild-type *FZD2*, ATF2 reporter was significantly activated compared to control (Fig. 6A). The G434V variant protein activated ATF2 to the same extent as wtFZD2 while P142L protein could not activate the reporter above basal levels (Fig. 6A).

When added in combination with recombinant WNT5A, primarily a non-canonical ligand, the ATF2 activation by wtFZD2 and G434V was maintained (Fig. 6B). However, the P142L variant which is in the cysteine-rich binding domain, did not activate ATF2 in the presence of WNT5A (Fig. 6B). This data is the first to show that the P142L variant is less effective at utilizing hWNT5A. We replicated these results in HEK293 cells (Fig. 6C,D). When we combined equimolar amounts of plasmids expressing wtFZD2 and either variants, there was no evidence of synergistic or antagonistic effects on the JNK/PCP pathway (Fig. 6E).

ROR2 is the main receptor for WNT5A (Ho et al., 2012; Nishita et al., 2010; Mikels et al., 2009; Oishi et al., 2003). Addition of plasmid containing mouse *Ror2* fails to activate ATF2 in presence of P142L variant (Fig. 6F). Both WNT5A and *Ror2* (Fig. 6G) on their own can effectively activate ATF2 (Gignac et al., 2023; Gignac et al., 2019). When added together with the variants, there is no change in activity compared to cells that were not transfected with FZD2 plasmid (Fig. 6G). This data implies that the JNK/PCP pathway activity is active as long as WNT5A and ROR2 homodimers are present. ROR2 homodimers do not seem to form in the absence of WNT5A. s in these experiments without the ligand, signaling induced by the FZD2 co-receptor (Fig. 6F). Overall, our data showed that that the P142L is inactive in both canonical and non-canonical WNT pathways (Fig. 6I). Moreover, P142L variant interferes activity of *ROR2* if there are low levels of WNT5A (Fig. 6F). On the other hand, G434V variant failed to activate the canonical pathway and behaved like the wild-type FZD2 in ATF2-reporter assay (Fig. 6H).

DISCUSSION

Craniofacial deformities are the main clinical presentation of RS. Majority of the genes causing RS lie in the non-canonical pathway except for DVL and *FZD2*. There are 10 FZD receptors in humans but interestingly only *FZD2* has been associated with pathogenesis of RS (Zhang et al., 2021; Wiese et al., 2018). By performing overexpression of wild-type or mutant forms of *FZD2* over endogenous chicken genome which continues to express the Gallus orthologue, our experiments reveal any putative dominant functions. In this study we report novel and distinct functional and biochemical effects of missense *FZD2* variants G434V (c.1300G>A) and P142L (c.425C>T).

FZD2-RS mutations inhibit ossification by dominantly repressing WNT canonical pathway

In our study, excess exogenous wt*FZD2* in frontonasal mass inhibited upper beak patterning and ossification. The embryos did not have any external defects which is similar to RS-*FZD2* individuals who have mild craniofacial features compared to other RS causing genes (Zhang et al., 2021). It is possible that a more detailed clinical exam with cephalometric radiographs would show skeletal deficiencies. There are a few case reports of RS patients that included head CT (computed tomography) scans. A child with an autosomal dominant *WNT5A* mutation had defective ossification of the frontal bone (Kaissi et al., 2020). Thus far head CT scans of RS-*FZD2* individuals have not been published.

In our study we studied a receptor FZD2, that acts in both canonical and non-canonical WNT pathways and found that intramembranous bone formation was inhibited to such an extent that there several bones failed to differentiate. These results of decreased intramembranous ossification are similar to another study from our lab where non-canonical WNT signaling was disrupted by misexpression of either wt*WNT5A* or $WNT5A^{C83S}$ a mutation that causes ADRS (Hosseini-Farahabadi et al., 2017). The penetrance of the bone inhibition phenotype in that study was significantly greater with the C83S variant. Similarly, in mouse studies, increased *Wnt5a* levels inhibited cranial bone formation (van Amerongen et al., 2012). Here the transgene containing *Wnt5a* was under the regulation of a tetracycline inducible promoter. Unfortunately, the interpretation of these over expression experiments is not straightforward. In our study we found that *FZD2* variants downregulated one of the main receptors mediating the JNK-PCP pathway, *ROR2*, which is consistent with loss of signaling in the JNK-PCP pathway. Patients with loss of function mutations in *ROR2* have autosomal recessive RS(van Bokhoven et al., 2000). On

the other hand, the luciferase assays using the ATF2 reporter showed that the levels of activity were similar in wtFZD2 and the G434 variant but that the P142L variant had failed to activate the reporter. We should have seen a difference in the severity of beak ossification phenotypes between the P142L variant and the other FZD2 viruses, but this was not the case. It is possible that variability in viral expression makes it difficult to measure differences. We also were unable to assay for another readout of changes in JNK-PCP signaling, changes in chondrocyte polarity. In the frontonasal mass chondrocytes are not stacked in a regular pattern like in Meckel's cartilage (Hosseini-Farahabadi et al., 2017) or in endochondral bones (Gignac et al., 2023; Gignac et al., 2019). The full extent of JNK-PCP signaling defects that may be caused by FZD2 variants is unresolved.

Another potential cause of the bone phenotype is that the levels of canonical WNT signaling are lower as shown by lower *CTNNB1* expression and lower STF luciferase activity. In addition, the two variant receptors are predicted to repress canonical WNT signaling through dominant negative actions. Paradoxically, we also see an increase in nuclear β-catenin in vivo which should signal increased canonical WNT signaling. It is possible that cells are sensing lower overall levels of β-catenin-mediated signaling and that increasing nuclear shuttling of β-catenin is triggered as part of a feedback loop. Our results where lower β-catenin signaling leads to agenesis of intramembranous bones are consistent with mouse studies that show a gain of canonical WNT signaling in Axin2-/- mice stimulates ossification in the calvaria. Taken together, the results support a loss of canonical WNT signaling as being the likely cause of the skeletal deficiencies in the beak.

In addition to WNT pathway, we showed a parallel downregulation of *BMP2*, *BMP7*, BMP antagonist *NOGGIN*, and *BMPER* suggesting that exogenous FZD2 interfered with BMP-mediated signaling. *BMPER* was consistently downregulated by all FZD2 viruses at stage 28 and stage 30 in vivo. *BMPER* (a homologue of Crossveinless in Drosophila) is a secreted protein shown directly regulate multiple BMP ligands, is crucial for in bone development. Reduced *BMPER* activity has inhibitory effects on osteogenic differentiation of MSCs in vivo and in vitro (Xiao et al., 2018). *Bmper*$^{-/-}$ mice have skeletal defects (Ikeya et al., 2006) while patients with loss-of-function mutations in BMPER have DSD (Diaphanospondylodysostosis), a rare congenital skeletal disorder (Braun et al., 2021). Based on our data, downregulation of BMP pathway may be one of the mechanisms contributing to the bone phenotype and needs further investigation. Overall,

we have shown that in vivo overexpression of wtFZD2 or RS-FZD2 expressing viruses in the chicken embryos face can downregulate WNT canonical and BMP signaling.

Specific and novel effects of the FZD2-P142 variant on signaling

The P142L variant affects the extracellular CRD domain of FZD2 (White et al., 2018). Mutations in the CRD of FZD proteins result in misfolded proteins and/or partially misfolded proteins termed as "disorders of FZ-CRD" (Milhem and Ali, 2019). The RS variant substitutes a lysine for a proline. Loss of a proline located internally in α-helices or β-sheets, could break the secondary structures, thus destabilizing the protein. The possibly of whether this substitution leads to disruption in protein stability is not determined. However, we demonstrated that the P142L did not activate the canonical pathway. Here, we characterized the effects of the P142L mutation, specifically affecting the CDR, on binding with WNT3A (canonical) and WNT5A (non-canonical) ligands (Komiya and Habas, 2008). We demonstrated that the P142L missense mutation specifically interferes with the FZD2-WNT5A interaction and supresses the ATF2 activity. The same P142L variant was able maintain canonical pathway activity in the presence of WNT3A. This suggests that substitution of proline with leucine at 142 position is crucial for WNT5A and not for WNT3A binding. The addition of plasmid coding for mouse Ror2 to wtFZD2 or the G434V variant significantly increased activity of the ATF2 reporter compared to parent plasmid controls. In contrast, addition of plasmid coding for mouse Ror2 in the presence of the P142L variant caused ATF2 activity to decrease and reach levels that were significantly lower than the parent plasmid controls. This suggests that when the P142L variant forms a heterodimer with ROR2 then non-canonical signaling is dominantly repressed. In RS phenotypes are very specifically concentrated in the face and limbs and perhaps it is these regions that happen to co-express ROR2 and FZD2 within the same cells. Finally, while the Ror2-Fz7-Wnt5a complex has been shown experimentally to activate the JNK-PCP pathway (Nishita et al., 2010), the involvement of FZD2 in a complex with ROR2 and the WNT5A ligand has not been investigated until now.

Effects of FZD2-G434V mutation

The second variant in our study, c.1301G>T, G434V, located in the third intracellular loop, is linked with majority of ADRS cases (Zhang et al., 2021; White et al., 2018). G434V variant was also associated with pathogenesis of autosomal dominant Omodysplasia type II (OMODII), a syndrome that phenocopies RS and contributes to ∼14% of all RS cases (Zhang et al., 2021; Nagasaki et al., 2018; Warren et al., 2018; Türkmen et al., 2017; Saal et al., 2015). Our data also

showed that the G434V mutation supresses canonical WNT activity and also exerts dominant negative effects on the activity of wtFZD2. As expected, we did not see effects of the mutation on interaction with WNT3A or WNT5A. Glycine 434 is highly conserved and is in a region that is essential for dishevelled binding (White et al., 2018; Tauriello et al., 2012). Surprisingly, the substitution of Glycine with Valine at position 434 did not alter DVL-binding and canonical pathway activity in our luciferase assays. Overall, we were able to show that the ADRS-FZD2 mutation has dominant negative effects on the canonical WNT pathway but that these effects are not mediated by changes in DVL1 binding.

What did we learn about FZD2 variants and the RS phenotypes?

Our study has clarified the signaling defects caused by missense variants located in near the C- or the N-terminal part of *FZD2*. Extending these results to the proband with the P142L and W377* variants of FZD2 (White et al., 2018), we predict a combination of loss of JNK-PCP signaling and decreased canonical WNT signaling. Furthermore, the dominant-negative function in the P142L allele in the canonical WNT pathway accentuates the loss of function of the W377* allele in this individual and could explain the combination of short stature and facial abnormalities. The 2 siblings with only the P142L variant have significant short stature but no obvious facial differences. Our data supports the hypothesis that the P142L variant is pathogenic due to decreased ability to signal in the canonical and non-canonical JNK-PCP pathways. Loss of JNK-PCP signaling could result in failure of limb chondrocytes to stack into columns leading to short stature.

Overall, we have shown for the first time that P142L substitution in FZD2-CDR, termed as a VUS, is pathogenic. We showed that P142L variant exerts dominant negative effects on activity of wtFZD2 and interferes with binding of WNT5A to receptors in the non-canonical JNK/PCP pathway.

MATERIALS AND METHODS:

Chicken embryo model:

White leghorn eggs (*Gallus Gallus*) obtained from the University of Alberta were incubated to the appropriate embryonic stages, based on the Hamilton Hamburger staging guide (Hamburger and Hamilton, 1992). All experiments were performed on prehatching chicken embryos which is exempted from ethical approval by the University of British Columbia Animal Care Committee and the Canadian Council on Animal Care.

Cloning of human *FZD2* constructs:

The open reading frame encoding human *FZD2* sequence was purchased from GeneCopoeia (Rockville, MD, clone #GC-S0193-B). Restriction-free cloning was used to add a C-terminal Flag-tag (DYKDDDDK) into wt*FZD2* vector (pShuttle) and a stop codon was added at the 3' end of the tag. Two autosomal dominant Robinow syndrome associated missense mutations (G434V, P142L) were knocked into the Flag-tagged wt*FZD2* (pShuttle) vector (Table S5). Flag-tagged wt or mutant FZD2 vectors *(*pShuttle) were then recombined into destination vectors (pcDNA 3.2 expression vector and RCAS retroviral vector) [LR clonase (Thermo Fisher #11791019)] as described (Hosseini-Farahabadi et al., 2017). GFP was not fused to the 5' end of FZD2 constructs due to the large size of GFP interfering with localization of FZD2 to the cell membrane. The small size of the FLAG-tag and its high hydrophilicity, tend to decrease the possibility of interference with protein expression and function (Einhauer and Jungbauer, 2001). To create the RCAS viruses, a Gateway compatible RCASBPY destination vector was used for recombination with the pShuttle vector using LR Clonase II (Loftus et al., 2001).

Growth of RCAS viral particles and viral titre:

Replication-Competent ASLV long terminal repeat (LTR) with a Splice acceptor (RCAS) plasmids DNA (2.5µg) of *GFP*, wt*FZD2* or mutant *FZD2* variants were transfected (Lipofectamine 3000, Thermo Fisher #L3000-008) into Douglas Foster-1 (DF-1) chicken cells (American Type Culture Collection, CRL-12203) as described (Logan and Francis-West, 2009). The *GFP* virus was provided by A. Gaunt and has been previously published by our lab (Gignac et al., 2023; Gignac et al., 2019; Hosseini-Farahabadi et al., 2017). Viruses encoding *GFP*, wt*FZD2* or mutant *FZD2* were passaged every three days. Viral stock was collected after 6 weeks of culture, concentrated, and stored at -80°C (Logan and Francis-West, 2009).

To determine the viral titre, 50-60% confluent DF1 fibroblasts were infected with serial dilution of 2µl of concentrated viral stock. 36 hours post incubation in virus, the cells were fixed in 4% paraformaldehyde for 30 mins. Immunocytochemistry was performed on virus treated cells with Group Associated Antigens (GAG), an antibody that recognises specific proteins in the RCAS virus. The cells were permeabilized for 30 mins with 0.1% Triton X-100 followed by blocking in a 10% goat serum and incubation with primary antibody overnight (Table 4). Fluorescence images were collected using Leica inverted microscope at 10x with a DFC7000 camera. Imaged cells were analyzed in ImageJ cell counter tool to determine the proportion of GAG positive cells (Fig. S7).

Chicken embryo injections

The frontonasal mass (anatomic region bounded by the nasal slits) of stage 15-16 chicken embryos (25-28 somites) was injected using a Picospritzer microinjector (General valve corp.). Infection of embryos with RCAS at stage 15-16 (E2.5) ensures maximum infection of facial prominences (Hosseini-Farahabadi et al., 2017; Geetha-Loganathan et al., 2014). Due to accessibility, all injections were made into the right frontonasal mass as the chick embryos turn on their left side during development. In the chicken embryos, the facial prominences form around stage 20, complex and temporally regulated patterning takes between stage 20-29. The skeletal derivatives of the frontonasal mass are fully patterned between stage 34-38. To study the effects of the *FZD2* viruses, we investigated stage 28 (E5.5, Table S4) and 38 (E12.5, Table S3) after performing overexpression of high titre (>2 x 10^8) *FZD2* viruses at stage 15 (E2.5). The location of *FZD2* viruses was only determined retrospectively on histological sections stained with a Group-associated antigens (GAG), an antibody that recognizes specific proteins in the RCAS virus or (Gignac et al., 2023; Gignac et al., 2019; Hosseini-Farahabadi et al., 2017; Geetha-Loganathan et al., 2014; Hosseini-Farahabadi et al., 2013; Chen et al., 2013; Kowalik and Hudspeth, 2011) antibody against the FLAG sequence (Gignac et al., 2023; Tetenborg et al., 2020) (Table S7).

Embryos grown till stage 38 were washed in 1x phosphate buffer saline (PBS) and fixed in 100% ethanol for 4 days, skinned, followed by incubation in 100% acetone for 4 days. The embryo heads were then stained with freshly made stain [0.3% Alcian blue 8GX in 70% ethanol (Sigma Aldrich), 0.1% alizarin red S (Sigma-Aldrich) in 95% ethanol, 1 vol 100% acetic acid, 17 vol 70% ethanol] for two weeks at room temperature. Post staining the skulls were washed in water and cleared in 2% KOH/20% glycerol solution for 4 days and then 50% glycerol for imaging. The

heads were stored 100% glycerol post imaging (Lee et al., 2001). The cleared heads were photographed for phenotyping using Leica DFC7000T microscope camera. Skeletal preparations from each virus type were analysed for the changes in the size or shape bones derived from the frontonasal mass, missing bones or qualitative reduction in ossification seen as reduced alizarin red stain (Table S2). Statistical analysis was done using contingency table, Chi-square test in Graph Pad Prism 10.0.2.

Primary cultures of frontonasal mass mesenchyme

Frontonasal mass mesenchymal cells were isolated from stage 24 chicken embryos, infected with *GFP* (control), wt*FZD2* or mutant *FZD2* (G434V or P142L) viruses (3µL), and plated into high density micromass cultures (2 x 10^7 cells/ml) as described (Underhill et al., 2014; Hosseini-Farahabadi et al., 2013; Richman and Tickle, 1992; Richman and Tickle, 1989). On day 4, 6 and 8, cultures were fixed in 4% paraformaldehyde for 30 mins and stained in wholemount staining. For detection of mineralization of cartilage with alkaline phosphatase stain, fixed cultures were incubated at room temperature in 100mM Tris for 30 mins (pH 8.3) followed by incubation in Naphthol AS-MX phosphate and Fast red violet LB salt stain for 1 hour in dark (Table S6). Next, the cultures were stained with 0.5% Alcian Blue in 95% EtOH: 0.1 M HCl (1:4) for detection of area occupied by cartilage as described (Underhill et al., 2014; Hosseini-Farahabadi et al., 2013). All the cultures were counterstained with 50% Shandon's Instant Hematoxylin. The stained cultures were photographed under standard illumination on a stereomicroscope (Leica #M125). Wholemount staining was performed on three biological and three technical replicates, and the experiment was repeated five times. A subset of RCAS infected 4% paraformaldehyde fixed cultures (day 6 and 8) were removed from the plate, embedded in 2% agarose (Sigma #A9539) and wax embedded. The cultures were vertically positioned in paraffin wax and cut into 7µm thick sections. Micromass cross-sectioned through the cartilage were used for histological (1% alcian blue and 0.1% Sirus Red F3B) (GFP n=6, wtFZD2 n=5, P142L n=5, G434V n=6) or immunofluorescence staining (n=4) for viral spread, WNT pathway and chondrogenic markers as described (Gignac et al., 2023; Gignac et al., 2019; Hosseini-Farahabadi et al., 2013)(Table S8).

Apoptosis and Cell proliferation

Apoptosis was analyzed using terminal deoxynucleotide transferase, dUTP nick-end labeling (TUNEL) staining at stage 28 (n=3), day 6 (n=3) and day 8 (n=3) cultures using the ApopTag Apoptosis Kit (Chemicon, S7101) and was detected using anti-digoxigenin tagged with fluorescein

as described (Hosseini-Farahabadi et al., 2017). For cell proliferation studies with BrdU (5-bromo-2'-deoxyuridine), 1µl of 10 mM BrdU (Sigma-Aldrich, B5002) was injected into the amniotic sac at stage 28 (Table S4) or diluted in culture media for micromass cultures (Hosseini-Farahabadi et al., 2017). Embryos/cultures were fixed in 4% paraformaldehyde 1-hour after BrdU treatment. All brightfield and fluorescence images were collected with a 20X objective on a slide scanner (3DHISTECH Ltd., Budapest, Hungary).

qRT-PCR on frontonasal mass in vivo and in vitro

Viral spread in the frontonasal mass was quantified using primers specific to human *FZD2* (primer set). Three biological replicates containing five to six pieces of the right half of the frontonasal mass pooled in each sample were harvested for each virus at stage 28 (E5.5) and stage 30 (E7.5). Similarly, three biological replicates containing pools of twelve micromass cultures per replicate were collected on day 6 and day 8. Total RNA was isolated from frontonasal masses using Qiagen RNAeasy kit (#75144, Toronto, Canada). Sybr green-based quantitive reverse transcriptase polymerase change reaction (Advanced universal SYBR® Green supermix; Bio-Rad #1725271) (qRT-PCR) was carried out using an Applied Biosystems StepOnePlus instrument. qRT-PCR cycling conditions were - 95°C for 10min, 40X (95°C for 5s, 60°C for 20 seconds). Analysis used human-specific primers for *FZD2* and avian primers for *FZD2, DVL1, LRP5, ROR2, WNT5A, CTNNB1, LEF1, ATF2, SOX9, TWIST1, TWIST2, RUNX2, SP7,BMP2, BMP7, BMPER, NOGGIN, MSX1* were used (Table S8). The expression of each biological replicate was normalized to 18s RNA (Applied Biosystems, 4328839) and then these ΔCt values were used to calculate the ΔΔCt relative to the average levels of expression of the gene in GFP-infected cultures. The ΔΔCt method was used to calculate relative fold-change expression between RS-*FZD2* infected frontonasal mass and *GFP* as described (Schmittgen and Livak, 2008). Statistical analysis was done with one-way ANOVA Tukey's post hoc test in GraphPad Prism 10.0.2.

Luciferase reporter assays

Transient transfections for luciferase assays were performed in HEK293T (0.15 x 10^6 cells/ml) (Gignac et al., 2023; Gignac et al., 2019) or using virus treated or untreated stage 24 frontonasal mass mesenchymal micromass cultures (2 x 10^7 cells/ml) as described (Geetha-Loganathan et al., 2014; Hosseini-Farahabadi et al., 2013). Cells were transfected with Lipofectamine 3000 (Invitrogen, L3000-008, Nunc 24-well plates #142475) transfection reagent. HEK293T cells were transfected 24h after plating (40-50% confluence). Micromass cultures were allowed to attach for

45 mins after plating and transfection reagents were added to the culture spot 30 mins prior to flooding the culture plate with micromass media. The following plasmids were used: control/empty (pcDNA3.2/V5-DEST), h*FZD2*, $FZD2^{P142L}$, $FZD2^{G434V}$, m*Ror2* (Addgene, #22613), single or in combinations (totalling to 0.2µg for HEK293 cells and 0.6µg for micromass cultures). Firefly reporter plasmids: SuperTopflash (STF; 0.2ug, Addgene plasmid #12456) and Activating Transcription Factor 2 (0.4ug; ATF2) (Ohkawara and Niehrs, 2011) along with Renilla luciferase was transfected for normalization (0.01µg). Recombinant Wnt3a (100 ng/ml, R&D, #5036-WN-010) or Wnt5a protein (100 ng/ml, R&D # 645-WN-010) was added 24h post transfection.

To measure the WNT canonical/β-catenin pathway and chondrogenic activity in micromass, the cultures were infected with 3µl of concentrated virus at the time of plating. 24h after plating, we performed transient transfection with either STF or SOX9 luciferase (pGL3 4x48) (Weston et al., 2002). Renilla luciferase was used as normalization control. Assay reading was done 48h after transfection representing day 3 of culture. The dual-luciferase reporter assay system (Promega #E1910) was used for all luciferase assays as described (Geetha-Loganathan et al., 2014). Luminescence activity was detected with a PerkinElmer Victor X2 Multilabel Microplate Reader at 1 s reading with OD1 filter. All data shown represents two to three independent experiments with three technical and three biological replicates carried out for each transfection mixture. Statistical analysis done using one-way ANOVA, Tukey's post hoc test in GraphPad Prism 10.0.2.

Image analysis and statistics

The thickness of the histological sections of day 6 and 8 micromass cultures for each experimental condition was measured 3 times per culture (technical replicate) and for 3 different cultures (biological replicates). The linear measurement annotation tool in CaseViewer (version 2.4) was used to collect measurements. The area of Alcian blue as well as the edges of the full culture were circumscribed with the polygon tool in CaseViewer to give the area stained with alcian blue/total area. Cell counts were done using the counter plugin in ImageJ. For in vivo analysis, the density of cells in the prenasal cartilage in all treated samples was quantified (100 x 100μm^2) and the average cell density was used to calculate the percent cells expressing nuclear β-catenin and BrdU. For micromass cultures, number of cells expressing TWIST, SOX9, nuclear β-catenin, or TUNEL was divided by the total number of Hoechst positive cells (500 x 200μm^2).

Proportion of positive cells was statistically analysed using one-way ANOVA with Tukey's posthoc test in GraphPad Prism 10.0.2.

Acknowledgements

We are grateful to Esther Verheyen for obtaining joint funding from CIHR for this work. the Developmental Studies Hybridoma Bank (IA, USA) for providing antibodies. We thank Dr. Janel Kopp for use of the Histech slide scanner for all chicken histology images. We acknowledge the excellent cell counting carried out by Dima Lim and Karen Chen.

Competing interests

The authors declare no competing or financial interests.

Author contributions

Conceptualization: S.S.T and J.M.R.; Methodology: S.S.T and K.F.; Formal analysis: S.S.T. and J.M.R. Investigation: S.S.T., K.F., J.M.R.; Resources: J.M.R.; Writing - original draft: S.S.T. and J.M.R.; Writing - review & editing: S.S.T. and J.M.R; Supervision: J.M.R.; Project administration: J.M.R.; Funding acquisition: E.M.V., J.M.R.

Funding

This work was funded by the Canadian Institutes of Health Research (grant PJT-166182 to J.M.R. and E.M.V.).

Data availability

All relevant data can be found within the article and its supplementary information.

REFERENCES

Riquelme, R., Li, L., Gambrill, A. and Barria, A. (2023). ROR2 homodimerization is sufficient to activate a neuronal Wnt/calcium signaling pathway. *J Biol Chem*, 105350.

Gignac, S. J., MacCharles, K. R., Fu, K., Bonaparte, K., Akarsu, G., Barrett, T. W., Verheyen, E. M. and Richman, J. M. (2023). Mechanistic studies in Drosophila and chicken give new insights into functions of DVL1 in dominant Robinow syndrome. *Dis Model Mech* **16**.

Zhu, X., Xu, M., Leu, N. A., Morrisey, E. E. and Millar, S. E. (2023). FZD2 regulates limb development by mediating beta-catenin-dependent and -independent Wnt signaling pathways. *Dis Model Mech* **16**.

Liegel, R. P., Michalski, M. N., Vaidya, S., Bittermann, E., Finnerty, E., Menke, C. A., Diegel, C. R., Zhong, Z. A., Williams, B. O. and Stottmann, R. W. (2023). Successful therapeutic intervention in new mouse models of frizzled 2-associated congenital malformations. *Development* **150**.

Zhang, C., Jolly, A., Shayota, B. J., Mazzeu, J. F., Du, H., Dawood, M., Soper, P. C., Ramalho de Lima, A., Ferreira, B. M., Coban-Akdemir, Z. et al. (2022). Novel pathogenic variants and quantitative phenotypic analyses of Robinow syndrome: WNT signaling perturbation and phenotypic variability. *HGG Adv* **3**, 100074.

Rim, E. Y., Clevers, H. and Nusse, R. (2022). The Wnt Pathway: From Signaling Mechanisms to Synthetic Modulators. *Annu Rev Biochem* **91**, 571-598.

Rogers, S. and Scholpp, S. (2022). Vertebrate Wnt5a - At the crossroads of cellular signalling. *Semin Cell Dev Biol* **125**, 3-10.

Conlon, C. J., Abu-Ghname, A., Raghuram, A. C., Davis, M. J., Guillen, D. E., Sutton, V. R., Carvalho, C. M. B. and Maricevich, R. S. (2021). Craniofacial phenotypes associated with Robinow syndrome. *Am J Med Genet A* **185**, 3606-3612.

Correns, A., Zimmermann, L. A., Baldock, C. and Sengle, G. (2021). BMP antagonists in tissue development and disease. *Matrix Biol Plus* **11**, 100071.

Zhang, C., Mazzeu, J. F., Eisfeldt, J., Grochowski, C. M., White, J., Akdemir, Z. C., Jhangiani, S. N., Muzny, D. M., Gibbs, R. A. and Lindstrand, A. (2021). Novel pathogenic genomic variants leading to autosomal dominant and recessive Robinow syndrome. *American Journal of Medical Genetics Part A* **185**, 3593-3600.

Lojk, J. and Marc, J. (2021). Roles of Non-Canonical Wnt Signalling Pathways in Bone Biology. *Int J Mol Sci* **22**.

Abu-Ghname, A., Trost, J., Davis, M. J., Sutton, V. R., Zhang, C., Guillen, D. E., Carvalho, C. M. B. and Maricevich, R. S. (2021). Extremity anomalies associated with Robinow syndrome. *Am J Med Genet A* **185**, 3584-3592.

Anthony, C. C., Robbins, D. J., Ahmed, Y. and Lee, E. (2020). Nuclear Regulation of Wnt/beta-Catenin Signaling: It's a Complex Situation. *Genes (Basel)* **11**.

Mazzeu, J. F. and Brunner, H. G. (2020). 50 years of Robinow syndrome, (ed.: Wiley Online Library.

Kaissi, A. A., Kenis, V., Shboul, M., Grill, F., Ganger, R. and Kircher, S. G. (2020). Tomographic Study of the Malformation Complex in Correlation With the Genotype in Patients With Robinow Syndrome: Review Article. *J Investig Med High Impact Case Rep* **8**, 2324709620911771.

Tetenborg, S., Wang, H. Y., Nemitz, L., Depping, A., Espejo, A. B., Aseervatham, J., Bedford, M. T., Janssen-Bienhold, U., O'Brien, J. and Dedek, K. (2020). Phosphorylation of Connexin36 near the C-terminus switches binding affinities for PDZ-domain and 14-3-3 proteins in vitro. *Sci Rep* **10**, 18378.

Roifman, M., Brunner, H., Lohr, J., Mazzeu, J. and Chitayat, D. (2019). Autosomal dominant Robinow syndrome. In *GeneReviews®[Internet]*: University of Washington, Seattle.

Gignac, S. J., Hosseini-Farahabadi, S., Akazawa, T., Schuck, N. J., Fu, K. and Richman, J. M. (2019). Robinow syndrome skeletal phenotypes caused by the WNT5AC83S variant are due to dominant interference with chondrogenesis. *Hum Mol Genet* **28**, 2395-2414.

Milhem, R. M. and Ali, B. R. (2019). Disorders of FZ-CRD; insights towards FZ-CRD folding and therapeutic landscape. *Mol Med* **26**, 4.

White, J. J., Mazzeu, J. F., Coban-Akdemir, Z., Bayram, Y., Bahrambeigi, V., Hoischen, A., van Bon, B. W. M., Gezdirici, A., Gulec, E. Y., Ramond, F. et al. (2018). WNT Signaling Perturbations Underlie the Genetic Heterogeneity of Robinow Syndrome. *Am J Hum Genet* **102**, 27-43.

Abramyan, J. and Richman, J. M. (2018). Craniofacial development: discoveries made in the chicken embryo. *Int J Dev Biol* **62**, 97-107.

Nagasaki, K., Nishimura, G., Kikuchi, T., Nyuzuki, H., Sasaki, S., Ogawa, Y. and Saitoh, A. (2018). Nonsense mutations in FZD2 cause autosomal-dominant omodysplasia: Robinow syndrome-like phenotypes. *American Journal of Medical Genetics Part A* **176**, 739-742.

Warren, H. E., Louie, R. J., Friez, M. J., Frías, J. L., Leroy, J. G., Spranger, J. W., Skinner, S. A. and Champaigne, N. L. (2018). Two unrelated patients with autosomal dominant omodysplasia and FRIZZLED2 mutations. *Clinical case reports* **6**, 2252.

Xiao, F., Wang, C., Wang, C., Gao, Y., Zhang, X. and Chen, X. (2018). BMPER Enhances Bone Formation by Promoting the Osteogenesis-Angiogenesis Coupling Process in Mesenchymal Stem Cells. *Cell Physiol Biochem* **45**, 1927-1939.

Wiese, K. E., Nusse, R. and van Amerongen, R. (2018). Wnt signalling: conquering complexity. *Development* **145**.

Hosseini-Farahabadi, S., Gignac, S., Danescu, A., Fu, K. and Richman, J. (2017). Abnormal WNT5A signaling causes mandibular hypoplasia in Robinow syndrome. *Journal of dental research* **96**, 1265-1272.

Nusse, R. and Clevers, H. (2017). Wnt/β-catenin signaling, disease, and emerging therapeutic modalities. *Cell* **169**, 985-999.

Stricker, S., Rauschenberger, V. and Schambony, A. (2017). ROR-Family Receptor Tyrosine Kinases. *Curr Top Dev Biol* **123**, 105-142.

Türkmen, S., Spielmann, M., Güneş, N., Knaus, A., Flöttmann, R., Mundlos, S. and Tüysüz, B. (2017). A novel de novo FZD2 mutation in a patient with autosomal dominant omodysplasia. *Molecular syndromology* **8**, 318-324.

White, J. J., Mazzeu, J. F., Hoischen, A., Bayram, Y., Withers, M., Gezdirici, A., Kimonis, V., Steehouwer, M., Jhangiani, S. N., Muzny, D. M. et al. (2016). DVL3 Alleles Resulting in a -1 Frameshift of the Last Exon Mediate Autosomal-Dominant Robinow Syndrome. *Am J Hum Genet* **98**, 553-561.

White, J., Mazzeu, J. F., Hoischen, A., Jhangiani, S. N., Gambin, T., Alcino, M. C., Penney, S., Saraiva, J. M., Hove, H., Skovby, F. et al. (2015). DVL1 frameshift mutations clustering in the penultimate exon cause autosomal-dominant Robinow syndrome. *Am J Hum Genet* **96**, 612-22.

Saal, H. M., Prows, C. A., Guerreiro, I., Donlin, M., Knudson, L., Sund, K. L., Chang, C.-F., Brugmann, S. A. and Stottmann, R. W. (2015). A mutation in FRIZZLED2 impairs Wnt signaling and causes autosomal dominant omodysplasia. *Human molecular genetics* **24**, 3399-3409.

Geetha-Loganathan, P., Nimmagadda, S., Fu, K. and Richman, J. M. (2014). Avian facial morphogenesis is regulated by c-Jun N-terminal kinase/planar cell polarity (JNK/PCP) wingless-related (WNT) signaling. *Journal of Biological Chemistry* **289**, 24153-24167.

Underhill, T. M., Dranse, H. J. and Hoffman, L. M. (2014). Analysis of chondrogenesis using micromass cultures of limb mesenchyme. *Methods Mol Biol* **1130**, 251-265.

Hosseini-Farahabadi, S., Geetha-Loganathan, P., Fu, K., Nimmagadda, S., Yang, H. J. and Richman, J. M. (2013). Dual functions for WNT5A during cartilage development and in disease. *Matrix Biology* **32**, 252-264.

Chen, J. W., Zahid, S., Shilts, M. H., Weaver, S. J., Leskowitz, R. M., Habbsa, S., Aronowitz, D., Rokins, K. P., Chang, Y., Pinnella, Z. et al. (2013). Hoxa-5 acts in segmented somites to regulate cervical vertebral morphology. *Mech Dev* **130**, 226-40.

Tauriello, D. V., Jordens, I., Kirchner, K., Slootstra, J. W., Kruitwagen, T., Bouwman, B. A., Noutsou, M., Rüdiger, S. G., Schwamborn, K. and Schambony, A. (2012). Wnt/β-catenin signaling requires interaction of the Dishevelled DEP domain and C terminus with a discontinuous motif in Frizzled. *Proceedings of the National Academy of Sciences* **109**, E812-E820.

Goodnough, L. H., Chang, A. T., Treloar, C., Yang, J., Scacheri, P. C. and Atit, R. P. (2012). Twist1 mediates repression of chondrogenesis by β-catenin to promote cranial bone progenitor specification. *Development* **139**, 4428-4438.

Valenta, T., Hausmann, G. and Basler, K. (2012). The many faces and functions of beta-catenin. *EMBO J* **31**, 2714-36.

Ho, H. Y., Susman, M. W., Bikoff, J. B., Ryu, Y. K., Jonas, A. M., Hu, L., Kuruvilla, R. and Greenberg, M. E. (2012). Wnt5a-Ror-Dishevelled signaling constitutes a core developmental pathway that controls tissue morphogenesis. *Proc Natl Acad Sci U S A* **109**, 4044-51.

van Amerongen, R., Fuerer, C., Mizutani, M. and Nusse, R. (2012). Wnt5a can both activate and repress Wnt/beta-catenin signaling during mouse embryonic development. *Dev Biol*.

Yu, H., Ye, X., Guo, N. and Nathans, J. (2012). Frizzled 2 and frizzled 7 function redundantly in convergent extension and closure of the ventricular septum and palate: evidence for a network of interacting genes. *Development* **139**, 4383-94.

Wang, Y., Song, L. and Zhou, C. J. (2011). The canonical Wnt/beta-catenin signaling pathway regulates Fgf signaling for early facial development. *Dev Biol* **349**, 250-60.

Ohkawara, B. and Niehrs, C. (2011). An ATF2-based luciferase reporter to monitor non-canonical Wnt signaling in Xenopus embryos. *Dev Dyn* **240**, 188-94.

Beiraghi, S., Leon-Salazar, V., Larson, B. E., John, M. T., Cunningham, M. L., Petryk, A. and Lohr, J. L. (2011). Craniofacial and intraoral phenotype of Robinow syndrome forms. *Clin Genet* **80**, 15-24.

Kowalik, L. and Hudspeth, A. J. (2011). A search for factors specifying tonotopy implicates DNER in hair-cell development in the chick's cochlea. *Dev Biol* **354**, 221-31.

Sato, A., Yamamoto, H., Sakane, H., Koyama, H. and Kikuchi, A. (2010). Wnt5a regulates distinct signalling pathways by binding to Frizzled2. *EMBO J* **29**, 41-54.

Person, A. D., Beiraghi, S., Sieben, C. M., Hermanson, S., Neumann, A. N., Robu, M. E., Schleiffarth, J. R., Billington, C. J., Jr., van Bokhoven, H., Hoogeboom, J. M. et al. (2010). WNT5A mutations in patients with autosomal dominant Robinow syndrome. *Dev Dyn* **239**, 327-37.

Yu, H., Smallwood, P. M., Wang, Y., Vidaltamayo, R., Reed, R. and Nathans, J. (2010). Frizzled 1 and frizzled 2 genes function in palate, ventricular septum and neural tube closure: general implications for tissue fusion processes. *Development* **137**, 3707-17.

Nishita, M., Itsukushima, S., Nomachi, A., Endo, M., Wang, Z., Inaba, D., Qiao, S., Takada, S., Kikuchi, A. and Minami, Y. (2010). Ror2/Frizzled complex mediates Wnt5a-induced AP-1 activation by regulating Dishevelled polymerization. *Mol Cell Biol* **30**, 3610-9.

Mikels, A., Minami, Y. and Nusse, R. (2009). Ror2 receptor requires tyrosine kinase activity to mediate Wnt5A signaling. *J Biol Chem* **284**, 30167-76.

Geetha-Loganathan, P., Nimmagadda, S., Antoni, L., Fu, K., Whiting, C. J., Francis-West, P. and Richman, J. M. (2009). Expression of WNT signalling pathway genes during chicken craniofacial development. *Dev Dyn* **238**, 1150-65.

Logan, C. and Francis-West, P. (2009). Gene transfer in avian embryos using replication-competent retroviruses. *Molecular Embryology: Methods and Protocols*, 363-376.

Angers, S. and Moon, R. T. (2009). Proximal events in Wnt signal transduction. *Nat Rev Mol Cell Biol* **10**, 468-77.

Komiya, Y. and Habas, R. (2008). Wnt signal transduction pathways. *Organogenesis* **4**, 68-75.

Biechele, T. L. and Moon, R. T. (2008). Assaying beta-catenin/TCF transcription with beta-catenin/TCF transcription-based reporter constructs. *Methods Mol Biol* **468**, 99-110.

Schmittgen, T. D. and Livak, K. J. (2008). Analyzing real-time PCR data by the comparative CT method. *Nature protocols* **3**, 1101-1108.

Mazzeu, J. F., Pardono, E., Vianna-Morgante, A. M., Richieri-Costa, A., Ae Kim, C., Brunoni, D., Martelli, L., de Andrade, C. E., Colin, G. and Otto, P. A. (2007). Clinical characterization of autosomal dominant and recessive variants of Robinow syndrome. *Am J Med Genet A* **143**, 320-5.

Brugmann, S. A., Goodnough, L. H., Gregorieff, A., Leucht, P., ten Berge, D., Fuerer, C., Clevers, H., Nusse, R. and Helms, J. A. (2007). Wnt signaling mediates regional specification in the vertebrate face. *Development* **134**, 3283-95.

Gordon, M. D. and Nusse, R. (2006). Wnt signaling: multiple pathways, multiple receptors, and multiple transcription factors. *J Biol Chem* **281**, 22429-33.

Carron, C., Pascal, A., Djiane, A., Boucaut, J. C., Shi, D. L. and Umbhauer, M. (2003). Frizzled receptor dimerization is sufficient to activate the Wnt/beta-catenin pathway. *J Cell Sci* **116**, 2541-50.

Oishi, I., Suzuki, H., Onishi, N., Takada, R., Kani, S., Ohkawara, B., Koshida, I., Suzuki, K., Yamada, G. and Schwabe, G. C. (2003). The receptor tyrosine kinase Ror2 is involved in non-canonical Wnt5a/JNK signalling pathway. *Genes to Cells* **8**, 645-654.

Weston, A. D., Chandraratna, R. A., Torchia, J. and Underhill, T. M. (2002). Requirement for RAR-mediated gene repression in skeletal progenitor differentiation. *J Cell Biol* **158**, 39-51.

Patton, M. A. and Afzal, A. R. (2002). Robinow syndrome. *J Med Genet* **39**, 305-10.

Dann, C. E., Hsieh, J. C., Rattner, A., Sharma, D., Nathans, J. and Leahy, D. J. (2001). Insights into Wnt binding and signalling from the structures of two Frizzled cysteine-rich domains. *Nature* **412**, 86-90.

Einhauer, A. and Jungbauer, A. (2001). The FLAG™ peptide, a versatile fusion tag for the purification of recombinant proteins. *Journal of biochemical and biophysical methods* **49**, 455-465.

Loftus, S. K., Larson, D. M., Watkins-Chow, D., Church, D. M. and Pavan, W. J. (2001). Generation of RCAS vectors useful for functional genomic analyses. *DNA Res* **8**, 221-6.

Lee, S.-H., Fu, K., Hui, J. and Richman, J. (2001). Noggin and retinoic acid transform the identity of avian facial prominences. *Nature* **414**, 909-912.

van Bokhoven, H., Celli, J., Kayserili, H., van Beusekom, E., Balci, S., Brussel, W., Skovby, F., Kerr, B., Percin, E. F. and Akarsu, N. (2000). Mutation of the gene encoding the ROR2 tyrosine kinase causes autosomal recessive Robinow syndrome. *Nature genetics* **25**, 423.

Bi, W., Deng, J. M., Zhang, Z., Behringer, R. R. and de Crombrugghe, B. (1999). Sox9 is required for cartilage formation. *Nat Genet* **22**, 85-9.

Ng, L. J., Wheatley, S., Muscat, G. E., Conway-Campbell, J., Bowles, J., Wright, E., Bell, D. M., Tam, P. P., Cheah, K. S. and Koopman, P. (1997). SOX9 binds DNA, activates transcription, and coexpresses with type II collagen during chondrogenesis in the mouse. *Dev Biol* **183**, 108-21.

Bell, D. M., Leung, K. K., Wheatley, S. C., Ng, L. J., Zhou, S., Ling, K. W., Sham, M. H., Koopman, P., Tam, P. P. and Cheah, K. S. (1997). SOX9 directly regulates the type-II collagen gene. *Nat Genet* **16**, 174-8.

Zhao, Z., Lee, C. C., Baldini, A. and Caskey, C. T. (1995). A human homologue of the Drosophila polarity gene frizzled has been identified and mapped to 17q21. 1. *Genomics* **27**, 370-373.

Hamburger, V. and Hamilton, H. L. (1992). A series of normal stages in the development of the chick embryo. *Developmental dynamics* **195**, 231-272.

Richman, J. M. and Crosby, Z. (1990). Differential growth of facial primordia in chick embryos: responses of facial mesenchyme to basic fibroblast growth factor (bFGF) and serum in micromass culture. *Development* **109**, 341-8.

Robinow, M., Silverman, F. N. and Smith, H. D. (1969). A newly recognized dwarfing syndrome. *Am J Dis Child* **117**, 645-51.

FIGURE LEGENDS

Figure 1: In vivo misexpression of FZD2 viruses into the upper jaw inhibits patterning and ossification: Schematic showing injection of RCAS viruses into the frontonasal mass (green) at stage 15 (E2.5). The development of the face was followed at stage 28 (E5.5) and further until full skeletal maturation at stage 38 (E12.5) (A). Contingency analysis of embryos injected with viruses coding for control GFP, wtFZD2, P142L or G434V, stained with alcian blue and alizarin red at stage 38 and analysed for missing bones or qualitative reduction in ossification of the upper beak bones using Chi Square test in GraphPad Prism 10.0.2.(B). Low- and high-power right lateral view of stage 38 embryos injected with GFP (C-C'), wtFZD2 (D-D'), P142L (E-E'), G434V (F-F') viruses stained with alcian blue and alizarin red skeletal preparation of. An embryo injected with GFP virus with green fluorescence localized in the upper beak showing accurate targeting (Inset in C'). Magnified right lateral and superior view of the upper beak shows that the normal size and shape of the upper beak in all viruses (C-F). The prefrontal bone (green dotted line) and the right nasal bone (white dotted line) was present in embryos injected with GFP virus (C') missing in majority of embryos injected with FZD2 viruses (D',E',F'). The premaxillary bone (black dotted line) was completely ossified in the GFP injected embryos (C'') but showed qualitatively reduced alizarin red staining in the embryos injected with FZD2 viruses (D'',E'',F''). The reduced cartilage stain in all the skulls is a technical error. Scale bar = 2mm. Key: et, egg tooth; f, frontal; fnm, frontonasal mass; j, jugal; ln, left nasal; mx, maxilla; md, mandible; n, nasal; prf, prefrontal; pmx, premaxilla; pnc, prenasal cartilage, q, quadrate; qj quadratojugal; rn, right nasal.

Figure 2: Early effects of the h*FZD2* viruses on the frontonasal mass: Embryos injected with RCAS viruses coding for GFP, wtFZD2 and FZD2 variants were collected on day 3 post injection (stage 28) and stained with anti-GAG antibody to determine viral spread. There was adequate viral spread in the frontonasal mass suggesting accuracy of targeting (A-D). Despite of the presence of virus, serial sections showed normal expression of early chondrogenic marker SOX9 (A'-D') in the prenasal cartilage area surrounded by differentiation TWIST1 positive mesenchymal cells (A''-D''). There was no effect of the viruses on cell proliferation shown by anti-BrdU antibody (A'''-D'''). The expression of canonical WNT pathway mediator nuclear β-catenin was slightly higher in embryos injected with FZD2 viruses compared to GFP (E-H', K). qRT-PCR analysis of RNA isolated from right half of the frontonasal mass infected with either GFP (control), human wtFZD2 or RS FZD2 variants. Three biological replicates with 5-6 frontonasal mass pieces pooled per

replicate. The expression of each biological replicate was normalized to 18s RNA and then these ΔCt values were used to calculate the ΔΔCt relative to the average levels of expression of the gene in GFP-infected cultures. The level of expression of human *FZD2* was measured with human-specific primers (I) and chicken specific primers for other WNT and BMP pathway genes analyzed (J). There was a 2-to-4.5-fold increase in level of h*FZD2* in FZD2 infected frontonasal. There was no change in the expression of g*FZD2* induced by the h*FZD2* viruses (I, J). Significant decreases in expression of g*CTNNB1* and g*BMPER* was caused by all FZD2 viruses. Individually, P142L variant downregulated gROR2, gBMP2, gBMP7, gNOGGIN while G434V variant downregulated gROR2 and gBMP2 (J). Statistical analysis done with one-way ANOVA, Tukey's post hoc test in GraphPad Prism 10.0.2. p*<0.05, **p<0.01, Scale bar in A = 100µm applies to B-D'', E'-H'; scale bar for E (high power) = 20µm, applies to F-H). Key: fnm, frontonasal mass; mxp, maxillary prominence, ns- not significant; pnc, prenasal cartilage.

Figure 3: In vitro misexpression of viruses containing hFZD2 variants inhibited chondrogenesis in frontonasal mass micromass cultures: Histological sections of day 6 cultures stained with alcian blue (glycosaminoglycan in cartilage) and picrosirius red (cartilage collagen). On day 6 all virus conditions formed Alcian blue positive cartilage sheets equally (A-D). Near-adjacent sections stained with the anti-GAG antibody showing viral spread in the cultures (E-H). Adjacent sections immunostained with type II collagen (COL2A1), a cartilage matrix protein (I-L). Histological sections of day 8 cultures showed reduced alcian blue and thickness in FZD2 infected cultures compared to GFP (M-P). Adequate viral spread was detected with immunostaining for anti-GAG and anti-FLAG antibodies (Q-T). All FZD2 infected cultures had weak COL2A1 expression (U-X). qRT-PCR analysis with hFZD2 and gFZD2 primers showed that all cultures infected with hFZD2 viruses has significantly higher h*FZD2* transcript level (Y). The levels of g*FZD2* remained unchanged (Z). Quantification of thickness of the histological sections was performed using CaseViewer software. Analysis of thickness revealed that the cultures infected with the hFZD2 variant viruses were significantly thinner as compared to GFP on day 8(AA) while all the FZD2 virus treated cultures were thinner compared to GFP on day 8 (AB). Quantification of percentage area occupied by cartilage showed significant reduction in all FZD2 viruses compared to GFP, the P142L virus significantly inhibited chondrogenesis even as compared to wtFZD2 and G434V viruses (AC). Chondrogenic capacity of virus infected cultures was quantified using 4x48 SOX9-luciferase reporter assay. Micromass cultures were transfected

with SOX9 luciferase reporter 24h after plating and reading was done 48h (day 3 of culture). Cultures infected with P142L virus showed significantly reduced SOX9-luc activity compared to other virus types (AD). Scale bar in A= 50µm applies to B-D, M-P, U-X Scale bar in E= 10µm applies to F-H, Q-T Scale bar in I = 50µm applies to J-L

Figure 4: Mutant hFZD2 variants increase expression of nuclear β-catenin and TWIST1 in day 8 micromass cultures: Sections of day 8 micromass cultures stained with anti-GAG antibody showing the viral spread in cultures (A-D). Immunostaining of adjacent sections with nuclear-β-catenin antibody (PY489) (E-H). Increased magnification of areas in white boxes is shown (E-H'). In cultures infected with GFP virus nuclear-β-catenin mainly localized in the nuclei of fibroblasts at the margins of the cultures (E, E'). wtFZD2 infected cultures showed lower expression of nuclear-β-catenin compared to the variants and the nuclear-β-catenin positive nuclei were distributed throughout the culture (F, F'). In cultures infected with P142L or G434V, nuclear-β-catenin was expressed abundantly in the nucleus of chondrocytes present in the cartilage sheets and in the undifferentiated cells at the margins of the cultures (G-H'). The number of cells expressing nuclear-β-catenin was quantified showing 40-60% positive cells in FZD2 variant infected cultures (M). Sections showing localization of TWIST1 positive nuclei in the COL2A1-poisitive cartilage extracellular matrix (I-L'). Intensity of COL2A1 appears to be weaker in cultures infected with hFZD2 viruses compared to GFP (I-L). The hFZD2 variant infected cultures have higher number of TWIST-positive nuclei compared to GFP and wtFZD2 (I'-L', O). WNT/β-catenin-mediated signaling in the virus infected cultures was quantified using Super Topflash (STF) luciferase reporter assay. Cultures were transfected with STF reporter 24h after plating and reading was done 48h (day 3 of culture). Cultures infected with P142L or G434V viruses showed significantly increased canonical WNT activity compared to GFP infected cultures (N). Scale bar in A = 10µm applies to B-D, E'-L', scale bar in E = 50 µm applies to F-H.

Figure 5: Effects of h*FZD2* variants of WNT canonical signaling pathway in frontonasal mass cultures and HEK293T cells: Super Topflash (STF) measures activity mediated by β-catenin. Transfection of hFZD2 variants to stage 24 frontonasal mass micromass cultures (A) or HEK293T cells (C) showed significantly lower activation of STF compared to wt*FZD2*. Addition of recombinant WNT3A (100ng/ml) to the cultures 24h post transfection increased the activity of *G434V* variant to the same level as wt*FZD2* but the *P142L* variant showed weak activity compared to wt*FZD2* and empty plasmid in the frontonasal mass cultures (B) In HEK293T cells, STF activity

increased for all *FZD2* plasmids in presence of WNT3A (D). Variants in combination with equimolar amounts of w*tFZD2* reduced the level of activation of STF (E). When added in combination with h*DVL1*, all *FZD2* plasmids showed equally increased STF activity which was significantly higher than the empty plasmid or h*DVL1* alone (F). Schematic showing normal activity of wt*FZD2* (G) and dominant negative effects of RS-*FZD2* variants (H) on the activity of wt*FZD2* in the canonical WNT pathway. One-way ANOVA, Tukey's post hoc test was used for all multiple comparisons. Key: A,B,C,D - 50% opacity colour signifies parent plasmid alone or in combination with FZD2 plasmids. E, F - 100% opacity signifies addition of wt*FZD2* or *DVL1* plasmids. For A and B, 0.6µg of plasmid (0.3 µg of plasmid without insert + 0.3µg of plasmid FZD2 plasmid) was used for transfection of frontonasal mass cultures; For C-F, 0.2µg of plasmid (0.1 µg of plasmid without insert/ hFZD2 + 0.1µg of hDVL1 plasmid); P values: *≤0.05, **≤0.01, ***≤0.001, ****≤0.0001, ns – not significant

Figure 6: Effects of h*FZD2* variants of WNT non-canonical signaling pathway in frontonasal mass cultures and HEK293T cells: Activating transcription factor 2 (ATF2) measures non-canonical WNT JNK PCP pathway activity. In stage 24 frontonasal mass micromass cultures *P142L* showed lower ATF2 activity compared to wt*FZD2* and *G434V* variant (A). Similarly, in HEK293 cells the activation of ATF2 was equivalent to empty plasmid but significantly lower compared to wt*FZD2* and *G434V* variant (C). Addition of recombinant WNT5A (100ng/ml) to the cultures 24h post transfection increased the activity of G434V variant to the same level as wt*FZD2* but the *P142L* variant showed weak activity similar to empty plasmid but lower than wt*FZD2* and *G434V* in the frontonasal mass cultures (B) and in HEK293T cells (D). Variants in combination with equimolar amounts of wtFZD2 showed equivalent ATF2 activation (E). When added in combination with non-canonical coreceptor mRor2, wtFZD2 and G434V showed similar ATF2 activation to each other and to Ror2 alone but P142L failed to activate ATF2 (F). Combination of h*FZD2*, m*Ror2*, and recombinant WNT5A (100ng/ml) showed comparable ATF2 activity for all FZD2 plasmids (G). Schematic showing normal activity of wtFZD2 and G434V variant (H) and loss-of-function in the P142L variant (I) in the non-canonical WNT pathway. One-way ANOVA, Tukey's post hoc test was used for all multiple comparisons. Key: A,B,C,D - 50% opacity colour signifies parent plasmid alone or in combination with FZD2 plasmids. E,F,G 100% opacity signifies addition of wt*FZD2* or Ror2 plasmids. For A and B, 0.6µg of plasmid (0.3 µg of plasmid without insert + 0.3µg of plasmid FZD2 plasmid) was used for transfection of frontonasal mass

cultures; For C-F, 0.2µg of plasmid (0.1 µg of plasmid without insert/ hFZD2 + 0.1µg of hDVL1 plasmid); P values: *≤0.05, **≤0.01, ***≤0.001, ****≤0.0001, ns – not significant.

Figure 7: Summary of signaling effects produced by wtFZD2 or Robinow syndrome associated FZD2 variants: Overexpression of the control/parent plasmid on top of gFZD2 (pink) showed basal level activity in both the canonical and non-canonical WNT pathways (A). Overexpression of wild-type human *FZD2* (blue) on top of gFZD2 caused significant elevated canonical and non-canonical reporter activation (B). The P142L variant (red) showed a dominant-negative effect by supressing the activity of the wtFZD2 in the canonical pathway. In addition, P142L failed to interact with *WNT5A* and *Ror2* and displayed an overall loss of function in JNK/PCP pathway (C). The G434V variant (yellow) also showed dominant-negative effect on the activity of the wtFZD2 but was able to activate ATF2 to the same extent as the wtFZD2 (D)

Figures

Figure 1

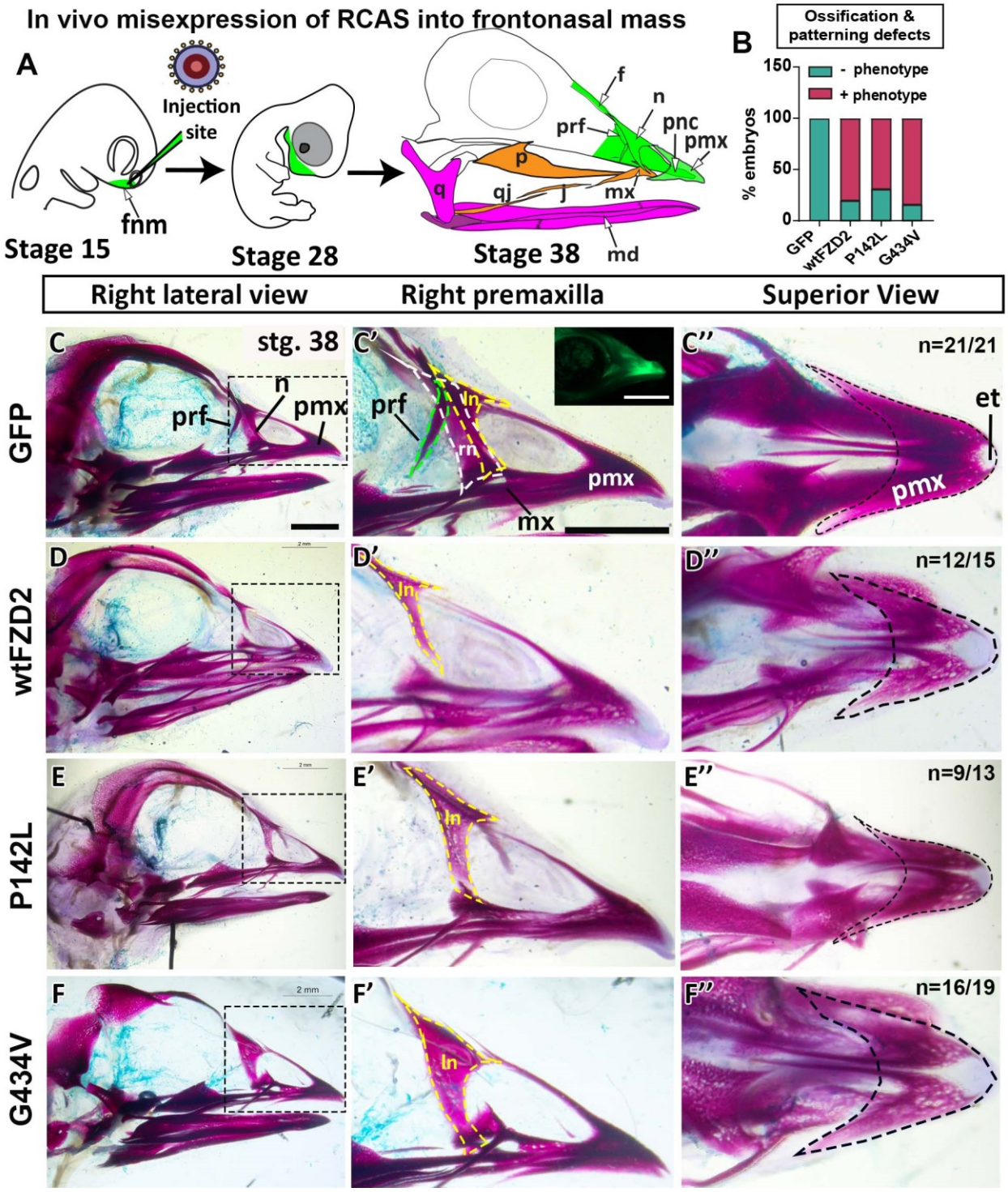

Figure 2

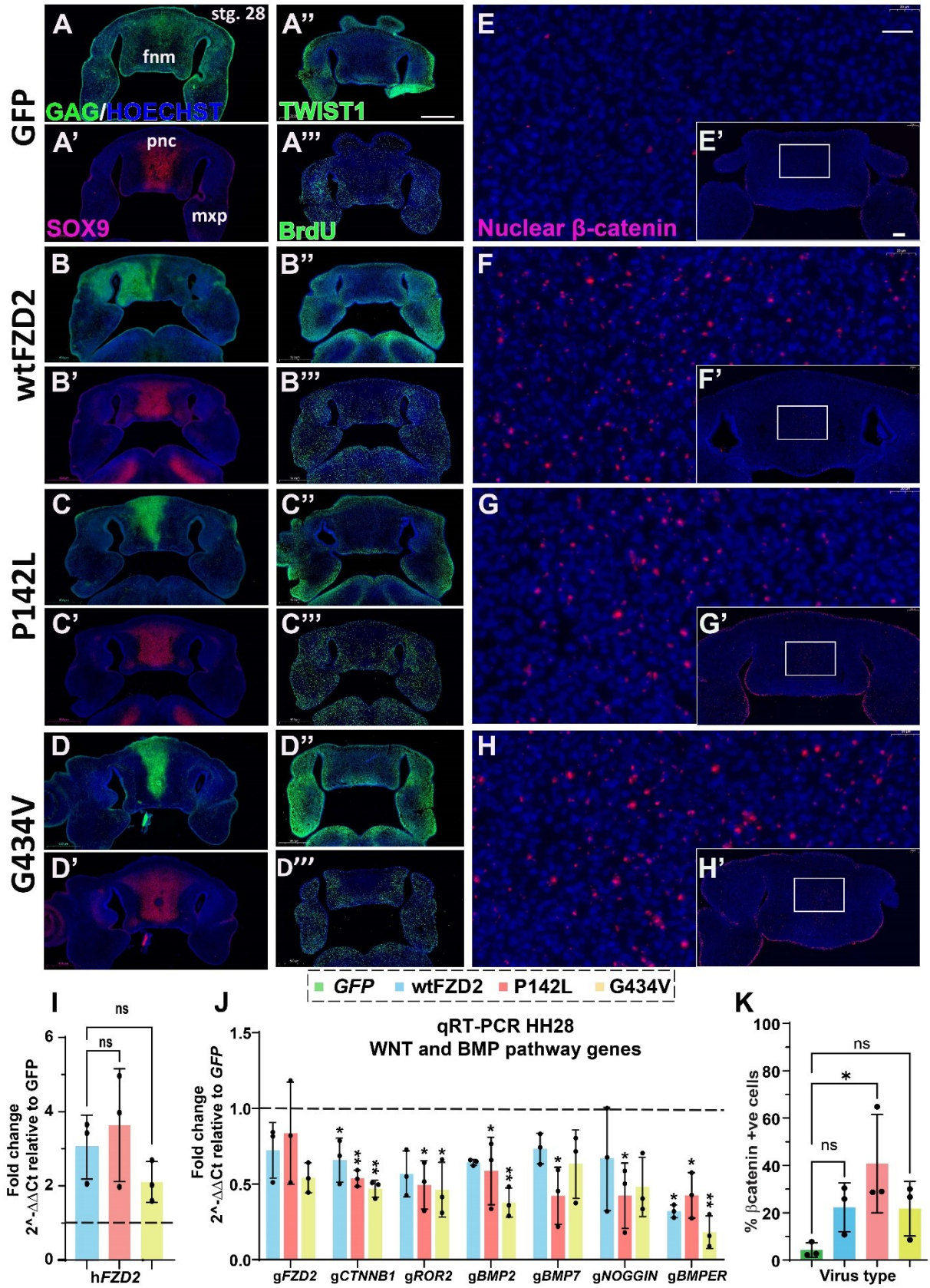
GFP
wtFZD2
P142L
G434V
A
stg. 28
fnm
GAG/HOECHST
A'
pnc
mxp
SOX9
A''
TWIST1
A'''
BrdU
E
E'
Nuclear β-catenin
B
B'
B''
B'''
F
F'
C
C'
C''
C'''
G
G'
D
D'
D''
D'''
H
H'
GFP
wtFZD2
P142L
G434V
I
ns
ns
Fold change
2^-ΔΔCt relative to GFP
hFZD2
J
qRT-PCR HH28
WNT and BMP pathway genes
Fold change
2^-ΔΔCt relative to GFP
gFZD2
gCTNNB1
gROR2
gBMP2
gBMP7
gNOGGIN
gBMPER
K
ns
*
ns
% βcatenin +ve cells
Virus type

Figure 3

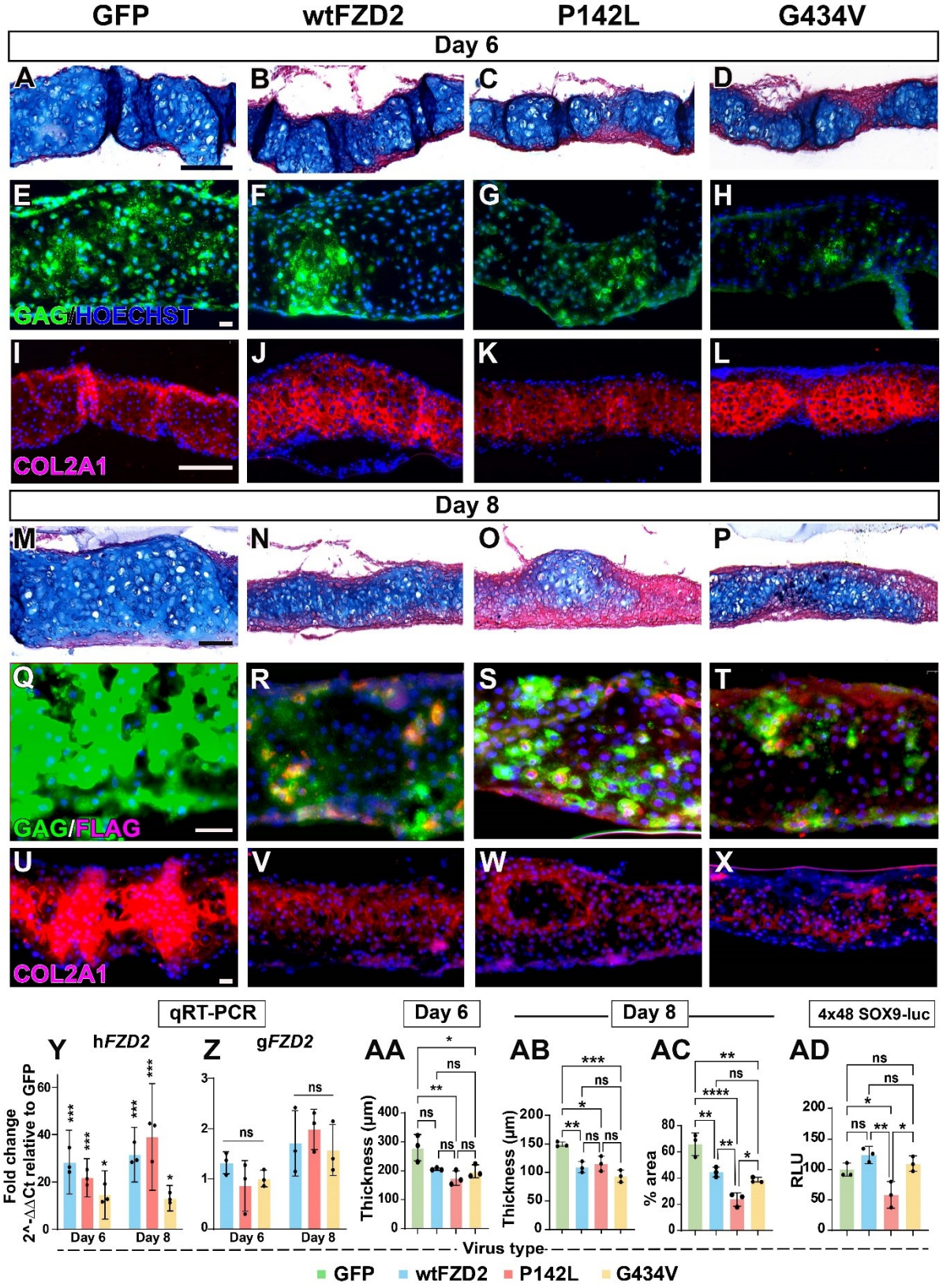
GFP
wtFZD2
P142L
G434V
Day 6
A
B
C
D
E
F
G
H
GAG/HOECHST
I
J
K
L
COL2A1
Day 8
M
N
O
P
Q
R
S
T
GAG/FLAG
U
V
W
X
COL2A1
qRT-PCR
Day 6
Day 8
4x48 SOX9-luc
Y
hFZD2
Fold change
2^-ΔΔCt relative to GFP
Day 6
Day 8
Z
gFZD2
AA
Thickness (µm)
AB
Thickness (µm)
AC
% area
AD
RLU
Virus type
GFP
wtFZD2
P142L
G434V

Figure 4

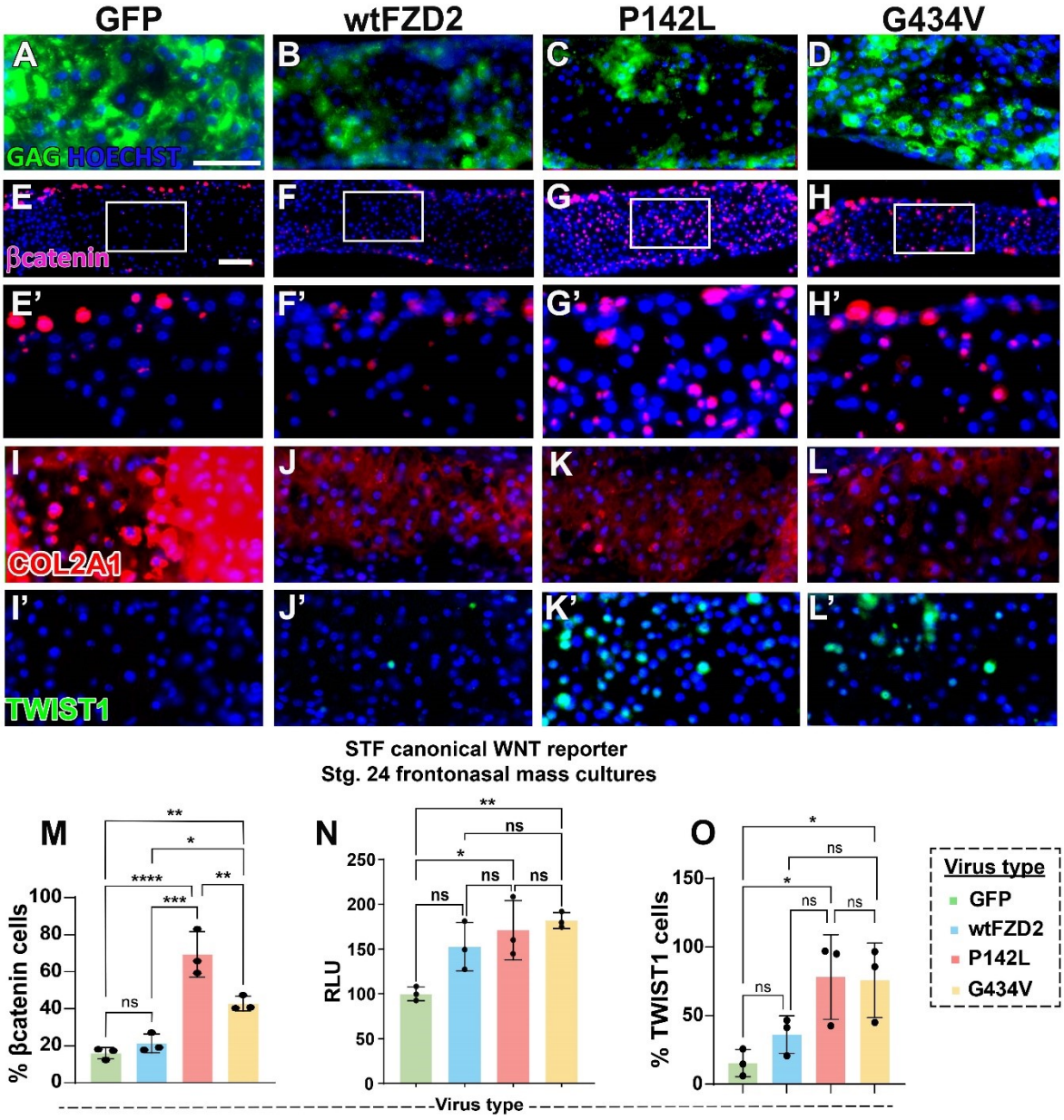
GFP
wtFZD2
P142L
G434V
A
B
C
D
GAG HOECHST
E
F
G
H
βcatenin
E'
F'
G'
H'
I
J
K
L
COL2A1
I'
J'
K'
L'
TWIST1
STF canonical WNT reporter
Stg. 24 frontonasal mass cultures
M
% βcatenin cells
N
RLU
O
% TWIST1 cells
Virus type
GFP
wtFZD2
P142L
G434V

Figure 5

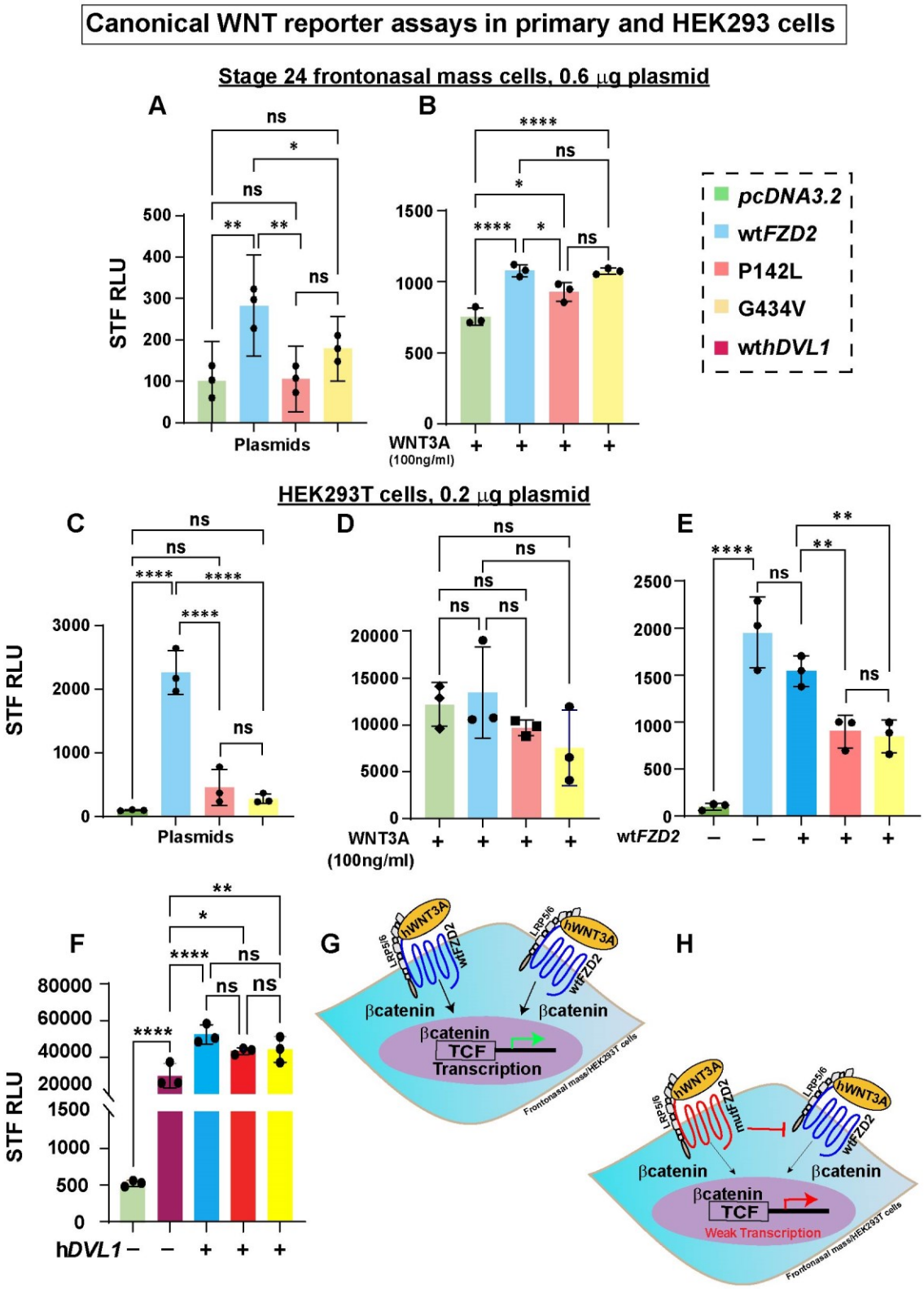
Canonical WNT reporter assays in primary and HEK293 cells
Stage 24 frontonasal mass cells, 0.6 μg plasmid
A
B
STF RLU
Plasmids
WNT3A
(100ng/ml)
pcDNA3.2
wtFZD2
P142L
G434V
wthDVL1
HEK293T cells, 0.2 μg plasmid
C
D
E
wtFZD2
F
hDVL1
G
H
hWNT3A
LRP5/6
wtFZD2
mutFZD2
βcatenin
TCF
Transcription
Weak Transcription
Frontonasal mass/HEK293T cells

Figure 6

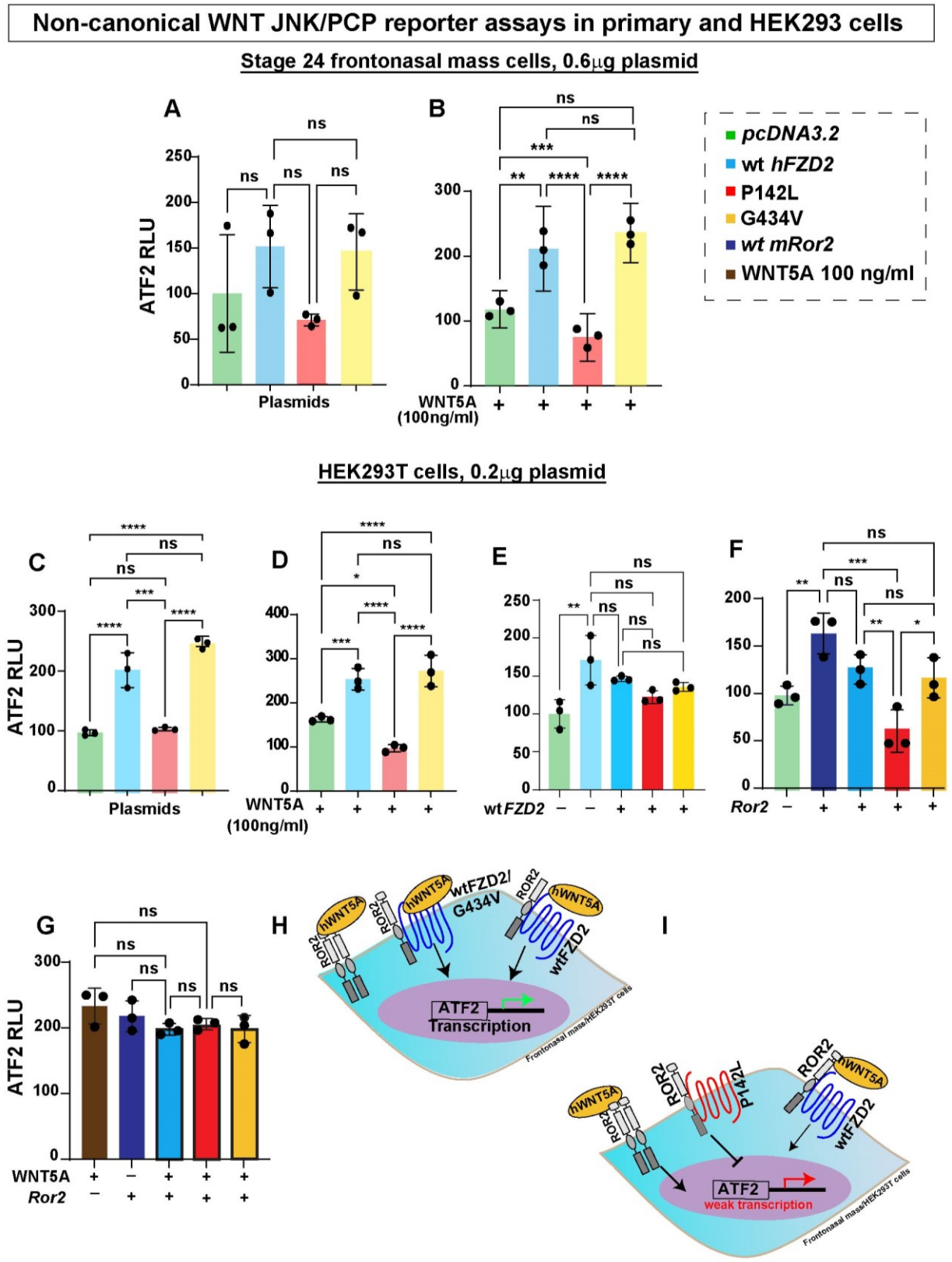
Non-canonical WNT JNK/PCP reporter assays in primary and HEK293 cells
Stage 24 frontonasal mass cells, 0.6μg plasmid
A
B
ATF2 RLU
Plasmids
WNT5A (100ng/ml)
pcDNA3.2
wt hFZD2
P142L
G434V
wt mRor2
WNT5A 100 ng/ml
HEK293T cells, 0.2μg plasmid
C
D
E
F
G
H
I
wtFZD2
Ror2
hWNT5A
ROR2
wtFZD2/ G434V
ATF2 Transcription
P142L
ATF2 weak transcription
Frontonasal mass/HEK293T cells

Figure 7

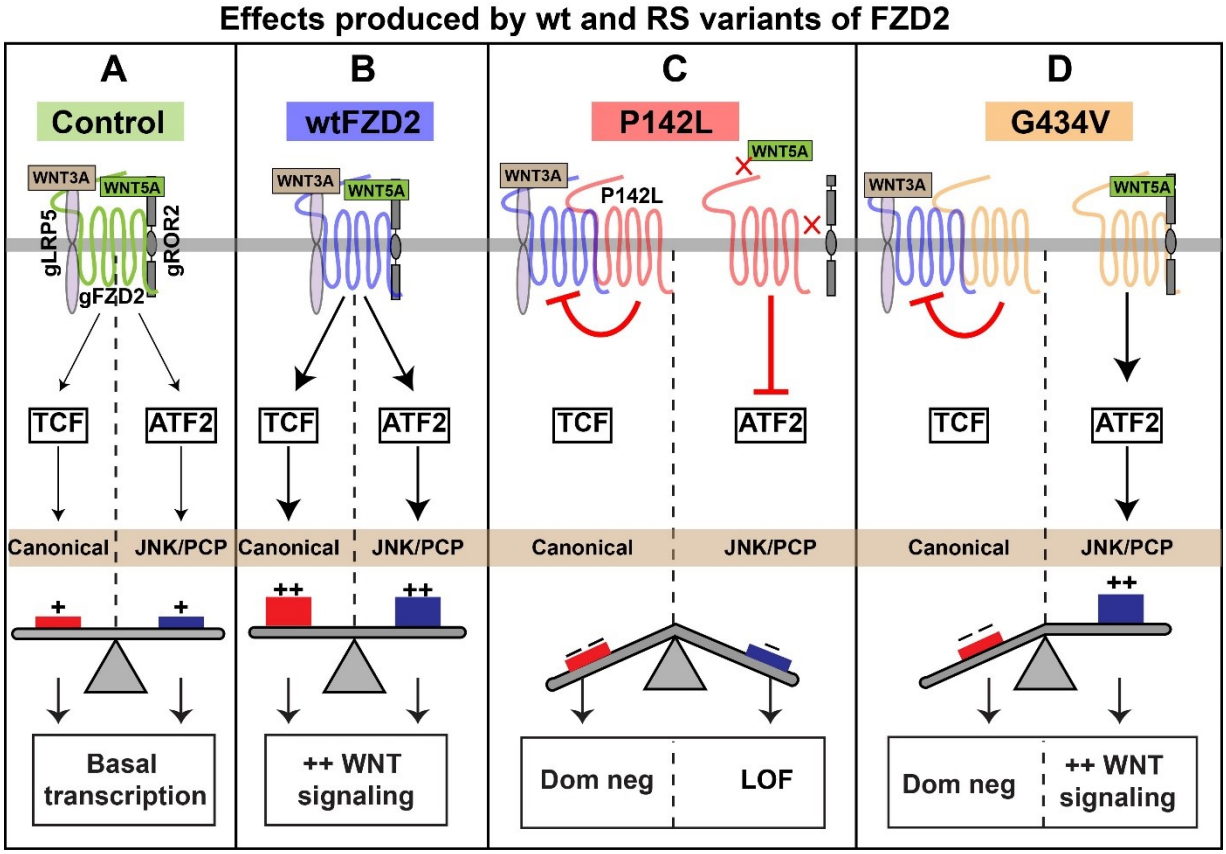
Effects produced by wt and RS variants of FZD2
A
Control
B
wtFZD2
C
P142L
D
G434V
WNT3A
WNT5A
gLRP5
gROR2
gFZD2
P142L
TCF
ATF2
Canonical
JNK/PCP
+
++
Basal transcription
++ WNT signaling
Dom neg
LOF